JGR Atmospheres

RESEARCH ARTICLE
10.1029/2019JD031544

Lightning and Associated Convection Features in the Presence of Absorbing Aerosols Over Northern Alabama

Tong Ren[1], Anita D. Rapp[1], John R. Mecikalski[2], and Jason Apke[3]

[1]Department of Atmospheric Sciences, Texas A&M University, College Station, TX, USA, [2]Atmospheric Science Department, University of Alabama in Huntsville, Huntsville, AL, USA, [3]Cooperative Institute for Research in the Atmosphere, Fort Collins, CO, USA

Key Points:
- Overall, aerosol optical depth and lightning flash rate do not show any significant linear relationship over northern Alabama
- Absorbing aerosols and storm area show a positive correlation in the low convective available potential energy regime
- The suppression of convection by absorbing aerosols and the convective available potential energy accumulation is presumably a link between absorbing aerosols and lightning

Supporting Information:
- Supporting Information S1

Correspondence to:
T. Ren,
tr7585@tamu.edu

Citation:
Ren, T., Rapp, A. D., Mecikalski, J. R., & Apke, J. (2019). Lightning and associated convection features in the presence of absorbing aerosols over northern Alabama. *Journal of Geophysical Research: Atmospheres*, *124*, 13,375–13,396. https://doi.org/10.1029/2019JD031544

Received 22 AUG 2019
Accepted 22 NOV 2019
Accepted article online 27 NOV 2019
Published online 14 DEC 2019

Abstract Many of the previous aerosol-convection/lightning enhancement studies are based on convective storms that occur in the presence of absorbing aerosols; such aerosols may impact deep convection through their microphysical and radiative effects. In this study, lightning flash rates (FRs) are analyzed together with aerosol optical depth (AOD) retrievals from the Moderate Resolution Imaging Spectroradiometer for summer storms during 2002–2015. Aerosol index retrievals from the Ozone Monitoring Instrument are used to separate nonabsorbing and absorbing aerosol cases. Statistical analyses are performed to test for significant sample differences and linear relationships between the AOD of case studies and the FRs, convective available potential energy, planetary boundary layer height, and low-level vertical wind shear to identify if evidence of regulation of storms by absorbing aerosols exists. Overall, AOD and FR do not show any significant linear relationship. When just observing absorbing aerosols, however, AOD and FR show a stronger (but still very weak) positive correlation. The weak correlation may be related to the absorbing aerosols' impact on convective available potential energy, which has a moderate linear correlation to AOD particularly when the instability is low, which implies some kind of convection or convective environment modification by absorbing aerosols. Although the planetary boundary layer height tends to decrease with increasing amount of absorbing aerosols, it is found that low-level vertical wind shear does not correlate with AOD for either absorbing or nonabsorbing aerosols. This result suggests little influence of the interaction between absorbing aerosols and turbulent mixing on storms.

1. Introduction

Lightning plays an important role in the Earth-atmosphere system and is one of the major causes of fire ignitions in wooded areas (e.g., Flannigan & Wotton, 1991; Rorig & Ferguson, 1999). Lightning-produced nitrogen oxides (LNO_x) can be transported by deep convection to the upper troposphere (UT) where their lifetimes are prolonged (Jaeglé, 2007). Increased LNO_x can lead to increased ozone production in UT, which may in turn warm the climate (Yuan et al., 2012). Siu et al. (2015) show that almost all the nitric oxide (NO) in the uppermost outflow layer is generated by lightning. Previous studies have suggested aerosols may impact deep convective storms—including single-cell thunderstorms (e.g., Li et al., 2008), tropical cyclones (e.g., Wang, Lee, et al., 2014), and midlatitude cyclones (e.g., Wang, Wang, et al., 2014)—and hence may also have an impact on the lightning activities associated with the deep convection.

Flash density is generally higher in a polluted environment than in a clean one in large continental regions (Altaratz et al., 2017). In a thunderstorm, charge is transferred between ice particles through their collisions in the presence of supercooled liquid water (Saunders et al., 2006; Takahashi, 1978). Differential sedimentation of graupel and small ice crystals in an updraft then results in charge regions. An adequately large volume of a strong updraft is necessary for cloud charge separation and lightning (Deierling et al., 2008; Deierling & Petersen, 2008; Schultz et al., 2017; Zipser, 1994). It has been suggested that aerosols may enhance lightning by modifying the cloud microphysics and local thermodynamics (Albrecht et al., 2011; Altaratz et al., 2010; Altaratz et al., 2014; Proestakis, Kazadzis, Lagouvardos, Kotroni, Amiridis, et al., 2016; Proestakis, Kazadzis, Lagouvardos, Kotroni, & Kazantzidis, 2016; Stolz et al., 2015; Stolz et al., 2017; Wang et al., 2011; Williams et al., 2002; Yuan et al., 2011). Increased aerosol particles lead to increased cloud condensation nuclei (CCN), resulting in a distribution of liquid cloud droplets with higher number concentrations and lower mean diameters, which lowers the efficiency of collision and coalescence (Albrecht, 1989;

Feingold, 2003) during the warm precipitation phase of a storm. As a consequence, cloud droplets that would have fallen to the surface may be later lifted above the freezing level as the convective system further develops, invigorating convection through release of latent heat (Andreae et al., 2004; Jenkins et al., 2008; Khain et al., 2005; Rosenfeld et al., 2008; Storer et al., 2014; van den Heever et al., 2006). Williams and Stanfill (2002) show that a global map of warm rain events and is essentially the inverse of the global map of lightning from Tropical Rainfall Measuring Mission lightning imaging sensor climatology. Thus, from a first-order perspective, aerosols have been hypothesized to be a potential key in the existence of the land-ocean lightning contrast through the convection invigoration process (e.g., Williams et al., 2002). Mansell and Ziegler (2013) successfully reproduced the convection invigoration by increased CCN in a simulation of a small multicell storm but found that the lightning production was sensitive to ice process parameterizations.

In addition, increased aerosol particles generally bring more ice nuclei (IN) whose role in the microphysical processes of mixed-phase clouds is thought to be important though is not currently understood (Seinfeld et al., 2016). Studies show the cloud glaciation temperature is dependent upon the ice-nucleating ability of aerosols (Hoose & Möhler, 2012; Murray et al., 2012; Roberts & Hallett, 1968). Heterogeneous ice nucleation occurs at warmer temperatures for effective IN, such as mineral dusts, biological species, and soot (Cziczo et al., 2004; DeMott, Cziczo, et al., 2003; DeMott, Sassen, et al., 2003; Levi & Rosenfeld, 1996; McCluskey et al., 2014; Richardson et al., 2007; Schaefer, 1949; Wilson et al., 2015). Model studies have suggested that increased IN concentration facilitates heterogeneous freezing and may result in increased ice concentrations (Li et al., 2013). Satellite observations have shown that dust aerosols favor ice particle formation within an altocumulus cloud that has a warmer base and top temperatures (Sassen et al., 2003). In the same study, Sassen et al. (2003) also suggest that deep convection may be affected by high loading episodes of African dust. Hence, it may be speculated that the aerosol lightning enhancement is due in part to adding not only more CCN but also more IN. Hereinafter, we call this potential impact of aerosols on lightning the CCN/IN mechanism, since both enhanced CCN and/or enhanced IN may lead to more supercooled water above the freezing level and enhanced noninductive charge separation.

From prior research, aerosol lightning enhancements are difficult to detect. Lightning activity was not significantly different between pristine and polluted environmental conditions in terms of CCN concentration in the premonsoon regime over the Amazon (Williams et al., 2002). Although thunderstorms occur more frequently in the relatively polluted environment during the Amazonian wet season (Albrecht et al., 2011), lightning flash rate did not increase with satellite aerosol optical depth (AOD) retrievals during the Amazonian dry season, when the loading of smoke aerosols is high (AOD $>$ 0.3) (Altaratz et al., 2010). Presumably, the high loading of smoke aerosols stabilizes the lower troposphere and suppresses the deep convective clouds (Altaratz et al., 2010). Based on the ground-based sun photometer AOD retrievals, Rodriguez et al. (2010) suggest no significant aerosol enhancement of lightning in austral summer over São Paulo, Brazil. Tan et al. (2016) show a negative correlation between monthly mean flash rate density and AOD in summers over Nanjing, China. Lightning is found more active in the workdays than at the weekends in the lee side of Paris, France (Coquillat et al., 2013). In reality, the development of a deep convective storm is often different from that of an idealized single cell as described in the CCN/IN mechanism. Changes during a period in a part of a convective system may be canceled or compensated for by an opposite change when the system is viewed as a whole (Grabowski, 2006; Grabowski & Morrison, 2011; Stevens & Feingold, 2009), making untangling aerosol effects on deep convection extremely difficult (Stevens & Feingold, 2009). Some modeling studies have suggested little influence of cloud droplet concentrations on the cloud buoyancy above the freezing level (Grabowski, 2015; Grabowski & Morrison, 2016), casting doubt on the convection invigoration process in the CCN/IN mechanism.

Among all types of aerosols, absorbing aerosols—such as black carbon and mineral dust—can absorb solar radiation (Huang et al., 2009; Li et al., 2010). Many previously discussed aerosol lightning enhancement and aerosol-convection invigoration studies are in the presence of absorbing aerosols. Ingested Saharan dust-absorbing aerosols appeared to invigorate the deep convection of the rain bands of a tropical storm (Jenkins et al., 2008). In the Intertropical Convergence Zone over the Atlantic where Saharan dust and African biomass burning-absorbing aerosols are carried by the prevailing easterlies, AOD showed strong positive correlations with cloud fraction and moderate negative correlations with cloud top pressure (Koren et al., 2005); such correlations did not appear to result from meteorological conditions or retrieval

artifacts (Koren et al., 2010). AOD and FR show a coincident trend in the presence of the low loading of smoke-absorbing aerosols (AOD < 0.2) over the Amazon region in the dry season (Altaratz et al., 2010). Smoke-absorbing aerosols have been observed by the space-borne lidar more frequently in lightning-active cases than nonlightning-active ones over the broader Mediterranean area (Proestakis, Kazadzis, Lagouvardos, Kotroni, Amiridis, et al., 2016). Enhanced lightning flash rate density has been observed over the main shipping lanes in the eastern Indian Ocean and the South China Sea, where increased absorbing aerosols from exhaust of ships are present (Thornton et al., 2017). In addition, previous studies have suggested that absorbing aerosols may impact the polarity of lightning flashes (Fernandes et al., 2006; Lyons et al., 1998; Murray et al., 2000). However, Smith et al. (2003) argue that the increased percentage of positive cloud-to-ground (CG) lightning flashes in the presence of smoke-absorbing aerosols is due to a dry and hot environment rather than increased CCN.

Absorbing aerosols can cool the surface and heat the atmosphere, stabilizing the lower troposphere and suppressing convection with an increased convection inhibition (Wang et al., 2013; Wong & Dessler, 2005); then, the convective available potential energy (CAPE) may be gradually accumulated, resulting in more intense convection later when the convection inhibition is overcome (Wang et al., 2013). This may also be a mechanism for aerosols to enhance lightning. Hereinafter, we call this hypothetical mechanism the CAPE mechanism. The hypothetical CAPE mechanism assumes that the presence of absorbing aerosols always acts to increase low-level stability and does not fully suppress eventual convection initiation. The reader should note that this assumption ignores the possibility that absorbing aerosols can exist in layers above the boundary layer and level of free convection, which could presumably reduce instability in the presence of more absorbing aerosols simply by modifying environmental lapse rates. Previous literature on the matter suggests that most aerosols are typically found in the boundary layer (e.g., Liu et al., 2009), which is why we make this assumption. In addition, absorbing aerosols suppress turbulence in the planetary boundary layer (PBL) (Ding et al., 2016; Dong et al., 2017; Li et al., 2017; Wilcox et al., 2016). The suppression of PBL turbulent mixing may reduce the PBL height (PBLH; Ding et al., 2016; Li et al., 2017) and enhance the low-level vertical wind shear (LLVWS), favorable for tornado occurrence in an already severe weather conducive environment (Saide et al., 2015). Saide et al. (2015) also suggest the potential impact of absorbing aerosols on nontornadic mesoscale phenomena through enhanced LLVWS, which is closely related to the number and lifetime of deep convective cells (e.g., Knupp & Cotton, 1982; Rotunno et al., 1988; Weisman & Rotunno, 2004). Hence, lightning activity may be linked to absorbing aerosols through the response of associated storms to enhanced LLVWS, which we call the PBL mechanism hereinafter. Again, this hypothetical mechanism assumes that the presence of absorbing aerosols always acts to stabilize the PBL, which will enhance LLVWS by reducing the altitude difference between the low-level jet maximum in the free atmosphere and the surface. These mechanisms imply that, in addition to the CCN/IN mechanism, the radiative effects may also contribute to enhanced lightning in the presence of absorbing aerosols by modification of the convection environment.

Based on the CAPE mechanism with the above assumptions, we hypothesize that if absorbing aerosols are present in a convective environment, the instability (CAPE) sampled will monotonically increase with increasing AOD. Further, based on the PBL mechanism with the above assumptions, we hypothesize that if the absorbing aerosols are present in a convective environment, then the LLVWS sampled monotonically increases with increasing AOD. The hypotheses in this study are meant to guide future works toward the possible linkages between aerosols and lightning flash rates. This study uses lightning, radar, and meteorological observations to test the hypotheses over northern Alabama. While it is not possible to fully disentangle the different aerosol-convection enhancement mechanisms with observations, we attempt to isolate conditions that would support the leading aerosol-convection theories. The objective of this study is to examine (1) the comparative associations of lightning with absorbing and nonabsorbing aerosols and (2) the aerosol situations, meteorological conditions, and ground-based radar reflectivity statistics in association with lightning variability to shed light on whether there is significant observational evidence for the aforementioned three mechanisms in the studied storms.

2. Data and Methodology

This study focuses on northern Alabama where long-term lightning data that dates back to 2002 are available from the North Alabama Lightning Mapping Array (NALMA) (Carey & Stough, 2016; Goodman

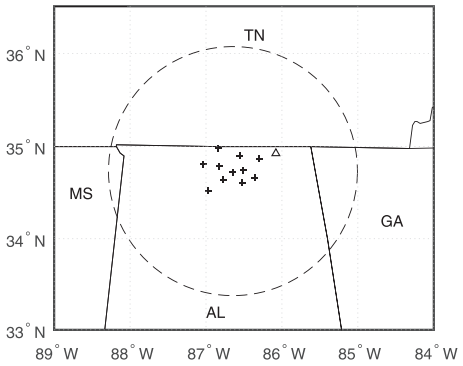

Figure 1. A map of the study area. The dashed circle is centered at the NALMA network with a radius of 150 km. AL, GA, MS, and TN are short for Alabama, Georgia, Mississippi, and Tennessee, respectively. The pluses are the detector locations of the NALMA. There were 10 NALMA stations before 2008, 11 in 2008, and 14 after 2008. The pluses in each panel mark the locations of the 11 NALMA stations through 2008. Not shown are three stations, one in Tennessee and two in Georgia, built after 2008. The triangle is the location of the KHTX site.

et al., 2005; Koshak et al., 2004). Lightning is most active in summer (June–August [JJA]) over northern Alabama (Albrecht et al., 2016; Christian et al., 2003), and hence, we focus on storm cases in the JJAs from 2002 to 2015. Because the location uncertainty of the detected lightning source increases with distance (Chmielewski & Bruning, 2016; Thomas et al., 2004), the study area is restricted to a circle centered at the NALMA network with a radius of 150 km (Figure 1), where the detection efficiency of the NALMA is above 90% (Chmielewski & Bruning, 2016). The LMA locates the intracloud and CG lightning sources by measuring how fast the impulsive very high-frequency radiation travels from the source to each of the stations, and archives lightning sources detected by at least six stations (Rison et al., 1999). The total lightning is used in this study, because intracloud and CG flashes are equally important from a cloud microphysics perspective. CG flashes only capture about 10% of total lightning in some cases (e.g., Boccippio et al., 2001). Considerable information may be lost if only CG flashes are examined, and it would be even more difficult to detect any relationship between lightning and aerosols. In this study, the lightning flashes detected by seven stations or more are used to further ensure the accuracy of flash locations, although a portion of the weak lightning signals are missed by this stricter criterion (Ren et al., 2018).

The overall aerosol loading is characterized using AOD retrievals (Levy, Remer, & Dubovik, 2007; Levy, Remer, Mattoo, et al., 2007) that also date back to 2002 from the Moderate Resolution Imaging Spectroradiometer (MODIS) on the Aqua satellite, which overpasses the study area in the early afternoon every day. MODIS AOD retrievals have been widely used in numerous meteorological and environmental studies (e.g., Niu & Li, 2012; Van Donkelaar et al., 2006). Absorbing aerosols are more capable of absorbing solar radiation than nonabsorbing aerosols. Satellite observations of ultraviolet radiation have been used to retrieve absorbing aerosols (Herman et al., 1999). Aerosol index (AI) retrievals that date back to 2005 from the Ozone Monitoring Instrument (OMI; Levelt et al., 2006) are used to discriminate between absorbing and nonabsorbing aerosols. The OMI is carried by the Aura satellite that also overpasses the study area in the early afternoon. The OMI AI retrieval algorithm is inherited from the Total Ozone Mapping Spectrometer (Herman et al., 1997), and the AI is derived from the backscattered radiance measurements at two wavelengths, 331 and 360 nm. The AI retrievals are available in both clear sky and cloudy conditions (Hsu et al., 1999; Hsu et al., 2003; Torres et al., 2007; Yu et al., 2012) and have been frequently used in studies related to absorbing aerosols (e.g., Chiapello & Moulin, 2002; Wilcox, 2010).

Figure 2 shows the long-term mean diurnal variation of the logarithm base 10 of flash rate, $\log_{10}(FR)$, over the study area in the JJAs from 2002 to 2015. The logarithmic transformation makes FR a more normal distribution. The lightning activity peaks in the late afternoon, in agreement with previous studies (Blakeslee et al., 2014; Chronis & Koshak, 2016; Williams & Heckman, 1993), shortly after the Aura and Aqua overpasses. The mean AOD is derived by averaging the available MODIS Collection 6 Level 2 AOD retrievals at a spatial resolution of 3 km (Levy et al., 2015; Levy et al., 2013) within the study area. At least 20 available retrievals are needed to ensure that the sample mean is adequately representative of the mean AOD over the study area (i.e., spatial representativeness). In addition, often thin and small clouds are not discerned by MODIS and are misinterpreted as clear sky conditions with heavy pollution (Altaratz et al., 2014). Therefore, only cases with mean AOD less than 1.0 are kept to remove possible false heavy pollution cases, although it should be noted that this criterion may also exclude some real heavy pollution cases (Van Donkelaar et al., 2011) and cannot remove the false cases completely. The mean AI is derived in the same way by averaging available AI retrievals within the study area using version 003 of the OMI Level 2 OMTO3 data (Bhartia, 2005). The spatial resolution of AI retrievals is 13 × 24 km, coarser than that of AOD retrievals. At least 10 available retrievals are needed to ensure spatial representativeness. Kim et al. (2007) used an AI threshold (AI_0) of 0.7 to partition the absorbing and nonabsorbing aerosols during the Atmospheric Brown Cloud–East Asian Regional Experiment campaign. Their AI_0 is adopted in this study. In each case, aerosols are considered absorbing if the mean AI > 0.7, and they are considered

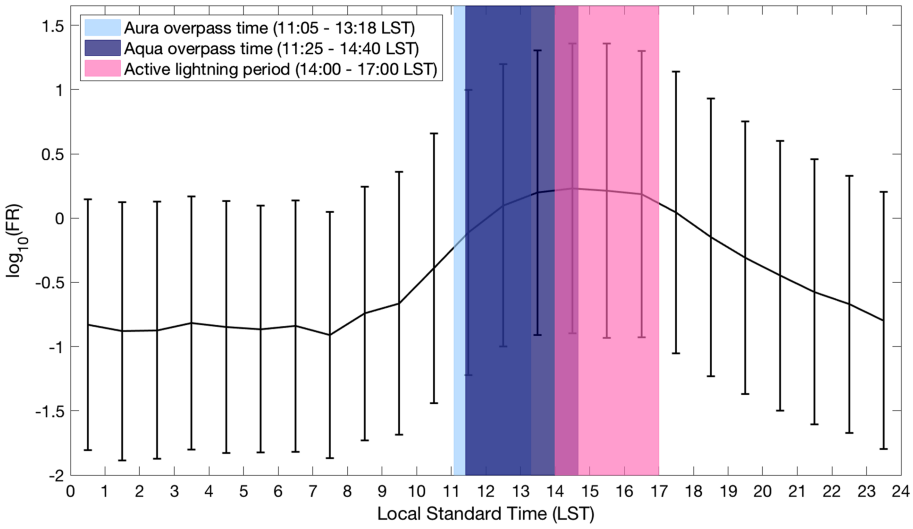

Figure 2. Long-term mean diurnal cycle of the logarithm of flash count, $\log_{10}$(FR), over northern Alabama in the JJAs from 2002 to 2015. The error bars show the standard deviations of $\log_{10}$(FR). The Aura satellite overpass time, the Aqua satellite overpass time, and the active lightning period are light blue-, dark blue-, and pink-shaded, respectively.

nonabsorbing if the mean AI $\leq$ 0.7. The probability distribution of AI appears to have multiple modes over Northern Alabama, and the subjectively selected AI_0 acts as a rough cutoff of the least absorbing mode (Figure 3).

Convection invigoration, the consequence of the potential aerosol impacts on deep convection and lightning, occurs when the enhanced conditional instability is released (e.g., Fan et al., 2008). It takes time for instability enhancements by aerosols to be converted into kinetic energy by deep convection. Therefore, this study focuses on describing the lightning features during 14:00–17:00 local standard time (LST) right after the satellite overpasses. The lightning flashes are counted over the study area during this active lightning period (180 min) to characterize the lightning activity of individual storms. Lightning FR in a given area is contributed by the lightning-producing deep convective area (LPDCA) and the flash rate per unit LPDCA (FR/LPDCA). Radar observations have been frequently used in identifying the lightning-producing storms (Bringi et al., 1997; Byers & Braham, 1949; Carey & Rutledge, 1996; Carey & Rutledge, 2000; Dye et al., 1986; Goodman et al., 1988; Larsen & Stansbury, 1974; MacGorman & Rust, 1998; Marshall & Radhakant, 1978; Schultz et al., 2011; Schultz et al., 2017; Williams et al., 1989). The Level 3 composite radar reflectivity data from the Hytop, Alabama (34.927°N, 86.080°W) KHTX WSR-88D are used in this study to estimate the LPDCA (Carey & Rutledge, 2000; Larsen & Stansbury, 1974). Every contiguous storm area

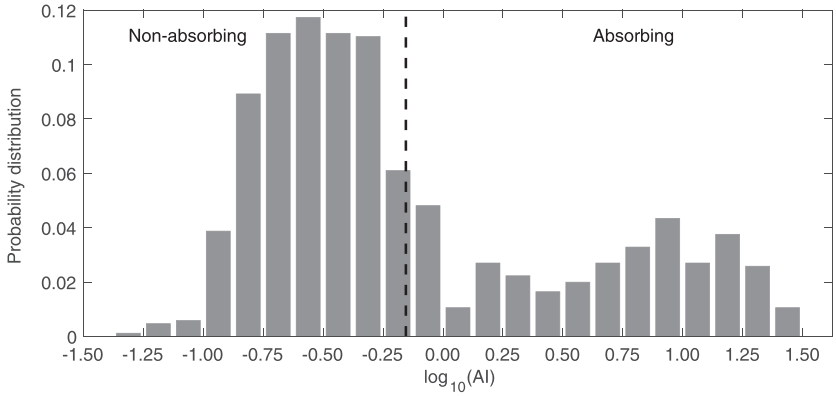

Figure 3. Probability distribution of the logarithm of mean AI, $\log_{10}$(AI), over northern Alabama in the JJAs from 2005 to 2015. The dashed line marks the selected AI threshold ($AI_0 = 0.7$) that separates the absorbing and nonabsorbing aerosols. The logarithmic transformation (base 10) makes each of the AI mode a more normal distribution.

where lightning flashes are present is considered an LPDCA if the composite radar reflectivity of each grid box in this area is greater than or equal to a threshold (30, 35, and 40 dBZ).

To examine if absorbing aerosols may have an impact on lightning and convection, the mean AOD is first correlated with FR for all storm cases and in the presence of absorbing and nonabsorbing aerosols, respectively; then it is correlated with the mean fraction of the LPDCA (F_{LPDCA}) over the study area and the mean FR/LPDCA during the active lightning period, respectively. The mean F_{LPDCA} is obtained by averaging the fractions for all the radar scans during the active lightning period. The FR/LPDCA is obtained by normalizing the FR during each radar scan by the detected LPDCA. The flashes over the study region within 4 min after the time of the scan are counted. The mean FR/LPDCA is then derived by averaging the normalized rates for all the scans during the active lightning period.

In addition to the aerosol loading, the lightning and associated convection features (LPDCA and FR/LPDCA) are related to meteorological conditions. Among other factors, lightning FR is thought to be regulated by both AOD and CAPE (Proestakis, Kazadzis, Lagouvardos, Kotroni, Amiridis, et al., 2016; Williams et al., 2002). The microphysics and dynamics are coupled in the context of aerosol invigoration of convection (Altaratz et al., 2014). Aerosol microphysical effects are sensitive to meteorological conditions (e.g., Albrecht et al., 2011; Fan et al., 2009; Storer et al., 2010; Storer et al., 2014; Zhao et al., 2018). Whether aerosols invigorate or suppress deep convection may depend upon the vertical wind shear (VWS) (Fan et al., 2009), which shapes the structure of convection (Malkus, 1949) and is one of the prominent synoptic features (Konrad, 1997). To compare the relative importance of aerosols and meteorological conditions in potential regulations of lightning and associated convection, FR, F_{LPDCA}, and FR/LPDCA are correlated with CAPE, LLVWS, and deep-layer VWS (DLVWS), respectively. The horizontal winds at 10 m and 850 hPa are used to calculate the LLVWS. The horizontal winds at 850 and 200 hPa are used to calculate the DLVWS (Konrad , 1997).

Aerosol particles primarily reside within the PBL and aerosol number concentration decreases exponentially with height above the PBL in general (Liu et al., 2009). Typically, aerosol light extinction in the PBL has a low value near the surface and increases with height with maximum at the PBL top (He et al., 2008). Therefore, although AOD is a column-averaged quantity, it is an approximate measure of the aerosol amount within the PBL. Thus, if the CAPE mechanism applies, then AOD and CAPE should show a positive correlation in the presence of absorbing aerosols. However, the reverse is not true, because other factors that may bring both high CAPE and high AOD cannot be ruled out. For instance, with a capping inversion atop the PBL, in addition to the CAPE accumulation, aerosols are expected to accumulate as well due partially to less vertical mixing. We therefore cannot fully prove the existence of the CAPE mechanism with the data in this study, we can only show observational evidence of the possibility of its existence. Similarly, if the PBL mechanism applies, then AOD and PBLH will show a negative correlation and AOD and LLVWS will show a positive correlation in the presence of absorbing aerosols, although the reverse is not true either. The CAPE mechanism is explored by correlating the AOD retrievals with the instantaneous Modern-Era Retrospective analysis for Research and Applications, version 2 (MERRA-2) $CAPE^{1/2}$ within the active lightning period (15:00 LST) and before (12:00 LST) for all the storm cases and the cases in the presence of absorbing aerosols, respectively. The PBL mechanism is explored by correlating the AOD retrievals with the mean MERRA-2 PBLHs and LLVWSs during 14:00–17:00 LST, respectively.

The CAPE, LLVWS, DLVWS, and PBLH data are derived from the MERRA-2, which assimilates the atmospheric aerosols with their radiative effects included in the atmospheric fields (Randles et al., 2016). In spite of the AOD constraint in the assimilation, the assimilation does not directly constrain the AI and hence is independent of the AI observations in this study (Randles et al., 2016). The 3-hourly instantaneous MERRA-2 Assimilated Meteorological Fields on model levels (GMAO, 2015b) are used to calculate the CAPE at 15:00 LST (21:00 UTC) that falls within the active lightning period. The gridded CAPE values are then averaged over the study area. The wind fields at 14:30, 15:30, and 16:30 LST (20:30, 21:30, and 22:30 UTC) from the 1-hourly time-averaged MERRA-2 Single-Level Diagnostics (GMAO, 2015d) are averaged to obtain the mean LLVWS between 10 m and 850 hPa and DLVWS between 850 and 200 hPa during the active lightning period. Then, the gridded time-averaged LLVWS and DLVWS values are averaged over the study area. The PBLHs at 14:30, 15:30, and 16:30 LST (20:30, 21:30, and 22:30 UTC) from the 1-hourly time-averaged MERRA-2 Surface Flux Diagnostics (GMAO, 2015c) are averaged to obtain the mean PBLH during the active lightning period. Then, the gridded time-averaged PBLH values are averaged over the

Table 1
Data Sources

Variables	Sources
Lightning flash	NALMA
AOD	Aqua MODIS Level 2 Collection 6 (3 km)
AI	Version 003 OMI Level 2 OMTO3
CAPE and freezing level	MERRA-2 Assimilated Meteorological Fields (model level)
LLVWS and DLVWS	MERRA-2 Single-Level Diagnostics
PBLH	MERRA-2 Surface Flux Diagnostics
Vertical profiles of *T*, *Td*, and wind	MERRA-2 Assimilated Meteorological Fields (pressure level)
Vertical profiles of aerosol types	Version 3.30 CALIOP Level 2 vertical feature mask
Composite radar reflectivity	WSR-88D (KHTX) Levels 2 and 3
Z and Z_{DR}	WSR-88D (KHTX) Level 2

entire study area. In numerical models, the PBLH is generally determined by examining where the bulk Richard number (Ri_b) exceeds a prescribed threshold (Zhang et al., 2014). The suppression of turbulent mixing by a capping inversion above the unstable boundary layer makes Ri_b exceed the threshold at a lower level, resulting in a reduced PBLH.

Last, a polluted case and a clean case are selected to illustrate the aerosol, convection, and meteorological situations in more detail with additional data sets, including (1) the vertical cross sections of radar reflectivity (Z) and differential reflectivity (Z_{DR}) from the KHTX WSR-88D Level 2 data; (2) vertical profiles of temperature (T), dew point temperature (Td), and horizontal wind at 12:00 LST from the 3-hourly instantaneous MERRA-2 Assimilated Meteorological Fields on pressure level (GMAO, 2015a); and (3) the aerosol type retrievals from the version 3.30 Level 2 vertical feature mask products (CALIPSO [Cloud-Aerosol Lidar and Infrared Pathfinder Satellite Observations] Science Team 2015; Vaughan et al., 2009) from the Cloud-Aerosol Lidar with Orthogonal Polarization (CALIOP), the lidar instrument on the CALIPSO satellite (Omar et al., 2009). Six predefined aerosol types are identified based primarily on CALIOP volume depolarization ratio measurements and associated extinction-to-backscatter ratios (lidar ratios) (Omar et al., 2009). Previous studies have suggested that absorbing aerosols either suppress or enhance the strength of capping inversion (Yu et al., 2002) and convection (Koch & Del Genio, 2010) depending on the vertical distribution of aerosol particles. The altitudes of the absorbing aerosol layers present in the selected cases are shown using the CALIPO aerosol type retrievals. The sources of all the data used in this study are documented in Table 1. The following results section starts with the correlation analysis of AOD and FR in presence of nonabsorbing and absorbing aerosols, followed by correlation analyses related to storm area and FR per storm. Then, the correlations between AOD and CAPE and between AOD and PBLH are presented. Last, a comparative study of a clean case, and a polluted case is shown.

3. Results

3.1. Absorbing Aerosols Versus Nonabsorbing Aerosols

A total of 592 storm-related lightning cases are found over northern Alabama in the summers during 2002–2015 when Aqua MODIS AOD retrievals are available. There are 173 cases during 2005–2015 dominated by absorbing aerosols based on an AI_0 of 0.7. Irrespective of the aerosol absorbance, the overall correlation coefficient between the mean AOD and $\log_{10}$(FR) for all the 592 cases is 0.107, smaller than that (0.246) for the 173 absorbing aerosol cases (Figure 4; A bin plot of Figure 4 is provided in the supporting information (Figure S2)). The p values (0.009 and 0.001) of the correlation coefficients (Figure 4) may be underestimated, because the effective degrees of freedom are supposed to be smaller than the sample size-based degrees of freedom estimation in the t test. Estimations of the effective degrees of freedom cannot be made without making additional assumptions. However, all the thunderstorm cases and associated AOD retrievals in this study are on different days and hence less dependent on one another. Moreover, the p value for the absorbing aerosol cases (0.001) is an order of magnitude smaller than the significance level (0.01). Therefore, the correlation for the absorbing aerosol case will likely pass the t test at the significance level of 0.01, if the effective degree of freedom is used in the significance test. The difference between the means of $\log_{10}$(FR) in the intervals $0.2 \leq AOD < 0.4$ and $0.4 \leq AOD < 0.6$ are statistically significant ($p = 0.002$) in the presence of absorbing aerosols (Figure S2). However, due to the smaller correlation coefficient (0.107) and the larger p value (0.009) for all the storm cases, we suggest that no significant linear relationship exists between AOD and FR in general, in contrast to Stolz et al. (2015) and Stolz et al. (2017). No significant correlation between AOD and FR shown in Figure 4 supports the previous modeling results (Grabowski, 2015; Grabowski & Morrison, 2016) that call the relevance of aerosols to convection invigoration into question, at least on a regional scale.

The weak positive correlation coefficient between AOD and $\log_{10}$(FR) that has a smaller p value in the presence of absorbing aerosols in Figure 4 may suggest that absorbing aerosols presumably have an impact on lightning. The presence of the weak correlation between the optical depth of absorbing aerosols and

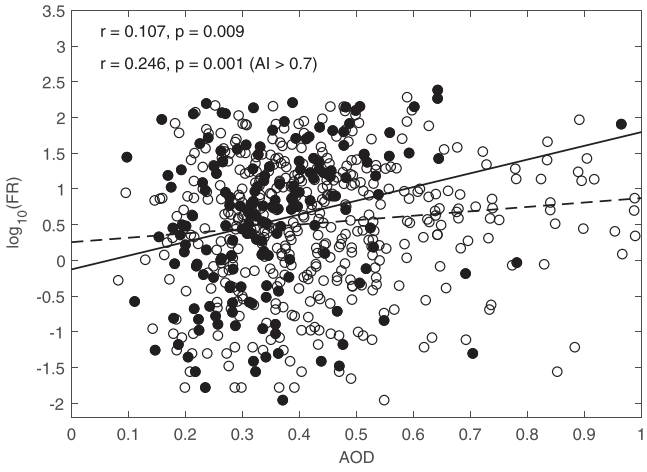

Figure 4. Scatterplot of $\log_{10}$(FR) versus the domain-averaged AOD during the JJAs from 2002 to 2015. Among the cases from 2005 to 2015, those mean AIs greater than 0.7 are marked by dots. The dashed line is the linear regression of $\log_{10}$(FR) on AOD for all the cases (circles and dots); the upper r and p are the corresponding correlation coefficient and *p* value, respectively. The solid line is the linear regression of $\log_{10}$(FR) on AOD for all the cases from 2005 to 2015 where AIs are greater than 0.7 (dots); the lower r and p are the corresponding correlation coefficient and *p* value, respectively. The Aqua MODS AOD retrievals date back to 2002; the OMI AI retrievals date back to 2005.

lightning FR is not sensitive to the selected AI_0 that separates absorbing and nonabsorbing aerosols. Table 2 documents correlation coefficients between AOD and $\log_{10}$(FR) for absorbing aerosols using different AI thresholds. The weak correlation coefficient between the optical depth of absorbing aerosols and lightning FR is always present, regardless of the selected AI_0. If the selected AI_0 is smaller or larger than 0.7, then the absorbing aerosols defined as such and FR will have a correlation coefficient that is not significantly different from the correlation coefficient between all (absorbing and nonabsoring) aerosols and FR (Table 2).

3.2. Correlations With Storm Area and Flash Rate Per Storm

Increased lightning FR can result from increased LPDCA or increased FR/LPDCA. Both aerosols and meteorological conditions correlate with the two parameters. Table 3 documents the correlation coefficients among the variables, where the LPDCA is defined using a composite radar reflectivity threshold of 30 dBZ. The correlation coefficients are also calculated with the LPDCA defined using the 35- and 40-dBZ thresholds, and the results are close and lead to the same conclusions (not shown). The logarithmic transformation (base 10) makes the mean F_{LPDCA} and the mean FR/LPDCA more normal distributions. We take the square roots of CAPE, LLVWS, and DLVWS to make the distributions more normal. The square root of CAPE is correlated to convective cloud updraft strength (Emanuel, 1994). Table 4 is the same as Table 3 except for the cases in the presence of absorbing aerosols.

Overall, $CAPE^{1/2}$ shows the strongest positive correlation with FR, and it correlates better with $\log_{10}$(FR/LPDCA) than with $\log_{10}(F_{LPDCA})$, suggesting that both the area of a convective system and the flash rate per unit storm area within the system are related to CAPE. However, the weak positive correlation between AOD and $\log_{10}$(FR) in the presence of absorbing aerosols appears to be primarily contributed by the association between the aerosol loading and the storm area rather than any association between the aerosol loading and the flash rate per unit storm area (Table 4). In agreement with the previous studies that have suggested the importance of updraft in determining FR (Deierling et al., 2008; Deierling & Petersen, 2008; Schultz et al., 2017; Zipser, 1994), the results in Tables 3 and 4 show that CAPE plays a more important role in regulating the flash rate per unit storm area. However, in agreement with the previous modeling studies (Grabowski, 2015; Grabowski & Morrison, 2016), aerosols do not appear to have a significant influence on the flash rate per unit storm area or updraft (Tables 3 and 4), which again casts doubt on the idealized single convective cell invigoration process described in the CCN/IN mechanism. Grabowski (2006) suggests a dichotomy of the process-level reasoning versus the system dynamics reasoning, depending on whether a single cloud or an ensemble of clouds is studied. It does not appear that the single cell invigoration process in the CCN/IN mechanism can be detected when ensembles of clouds are studied (Tables 3 and 4), which is in agreement with Grabowski (2006). Previous modeling studies of ensembles of clouds have suggested enhanced low-level convergence and secondary convection (e.g., Khain et al., 2005; Lee & Feingold, 2010), which may be a potential link between aerosols and storm area.

Table 2
Correlation Coefficients between AOD and $\log_{10}$(FR) in the Presence of Absorbing Aerosols (r_a, AI > AI_0) Using Different AI Thresholds (AI_0) and Z Test-Based p Values of the Differences Between the Correlation Coefficients and That for All the Storm Cases

AI_0	0.4	0.5	0.6	0.7	0.8	0.9	1.0
r_a	0.180**	0.235**	0.234**	0.246**	0.222**	0.238**	0.238**
p value	0.169	0.055	0.060	0.050	0.093	0.067	0.071

**t test statistic at a significance level of 0.01.

Table 3
Correlation Coefficients Among the Variables for All the Cases

	AOD	$CAPE^{1/2}$	$LLVWS^{1/2}$	$DLVWS^{1/2}$
$\log_{10}(FR)$	0.107**	0.467**	0.089*	−0.224**
$\log_{10}(F_{LPDCA})$	0.168**	0.297**	0.312**	−0.092**
$\log_{10}(FR/LPDCA)$	−0.127**	0.378**	−0.219**	−0.260**

*t test statistic at a significance level of 0.05. **t test statistic at a significance level of 0.01.

The weak positive correlation between the loading of absorbing aerosols and the storm area may not be readily explained by the convection invigoration as described in the CCN/IN mechanism, nor by the previously reported enhanced low-level convergence and secondary convection (e.g., Khain et al., 2005; Lee & Feingold, 2010). To the best of our knowledge, none of the previous studies have suggested absorbing aerosols are more efficient CCN than nonabsorbing aerosols. As efficient IN, mineral dust aerosols that are absorbing aerosols may potentially influence storms (Sassen et al., 2003); however, increased IN cannot be straightforwardly linked to increased storm area due to the limited knowledge of mixed-phase clouds. Moreover, it is not evident that the identified absorbing aerosols in this study necessarily consist of efficient ice-nucleating particles. However, the CAPE and PBL mechanisms presumably apply with the weak correlation between AOD and $\log_{10}(F_{LPDCA})$ in the presence of absorbing aerosols. Moreover, the CAPE and PBL mechanisms are not suggested based on a single convective cell and hence the necessary conditions of the two mechanisms can be examined by studying ensembles of clouds.

Absorbing aerosols absorb the incident solar radiation and prevent it from reaching the surface, cooling the surface and heating the layer above. This helps maintain a capping inversion that can suppress the turbulent mixing in the unstable PBL (Wilcox et al., 2016) and convection (Wong & Dessler, 2005) and result in a decreased PBLH (Ding et al., 2016; Dong et al., 2017). The suppression of convection can lead to the accumulation of CAPE and more intense storms later when convection is triggered (Wang et al., 2013). Previous studies have suggested that storm area may play an important role in determining the actual convective intensity of the storm (e.g., Williams et al., 2005; Williams & Stanfill, 2002). The CAPE mechanism may link increased absorbing aerosols to more intense storms that often have more widespread areas. F_{LPDCA} and FR/LPDCA generally do not show any significant correlation (not shown). In addition to CAPE accumulation, the suppression of turbulent mixing can also enhance the LLVWS (Saide et al., 2015), which can in turn facilitate the turbulent mixing over the surrounding area and hence potentially trigger deep convection nearby. The interaction of cold pools and enhanced LLVWS plays a key role in new cell formation in convective systems (Knupp & Cotton, 1982; Rotunno et al., 1988; Weisman & Rotunno, 2004). Such a mechanism may also link increased absorbing aerosols to increased storm area.

In addition, as documented in Tables 3 and 4, LLVWS shows a weak positive correlation with F_{LPDCA}, suggesting that more widespread storms are often associated with stronger LLVWS. DLVWS shows a relatively weak correlation with FR (Tables 3 and 4). Its correlation is more negative with the FR/LPDCA than with the F_{LPDCA} (Tables 3 and 4). The results suggest that enhanced DLVWS above the PBL is associated with reduced FR per unit storm area, which may be due to the negative association between DLVWS and CAPE (not shown). Vertical momentum transport in a mesoscale convective complex tends to reduce the DLVWS as convection intensifies (Wu & Yanai, 1994). Together, the results in Tables 3 and 4 suggest that the weak correlation between optical depth of absorbing aerosols and storm area may be contributed by the radiative effect of absorbing aerosols, but it should be always noted that observational correlation analysis cannot rule out other unknown factors that may impact variables examined simultaneously. The influence of some known factor on the examined variables may be reduced, if the variation of the factor is controlled in the analysis. The next section will try to isolate the aerosol effect from the strong influence of CAPE

Table 4
Correlation Coefficients Among the Variables for All the Cases in the Presence of Absorbing Aerosols

	AOD	$CAPE^{1/2}$	$LLVWS^{1/2}$	$DLVWS^{1/2}$
$\log_{10}(FR)$	0.246**	0.472**	0.098	−0.317**
$\log_{10}(F_{LPDCA})$	0.265**	0.290**	0.348**	−0.168*
$\log_{10}(FR/LPDCA)$	0.078	0.389**	−0.264**	−0.300**

*t test statistic at a significance level of 0.05. **t test statistic at a significance level of 0.01.

3.3. Categorized CAPE

As documented in Tables 3 and 4 and in agreement with previous studies (e.g., Williams et al., 2002), CAPE appears to be more influential in determining the FR of a storm, particularly the FR/LPDCA. The potential impacts of aerosols on lightning may be more detectable, if CAPE is categorized, that is, minimizing the CAPE effect on lightning. The storm cases are roughly grouped into the low, median, and high $CAPE^{1/2}$ regimes using a half standard deviation below and above the mean of $CAPE^{1/2}$, $\mu_{CAPE} \pm \sigma_{CAPE}/2$. The subjectively selected thresholds have been used in previous analytical studies, including the classification of the El

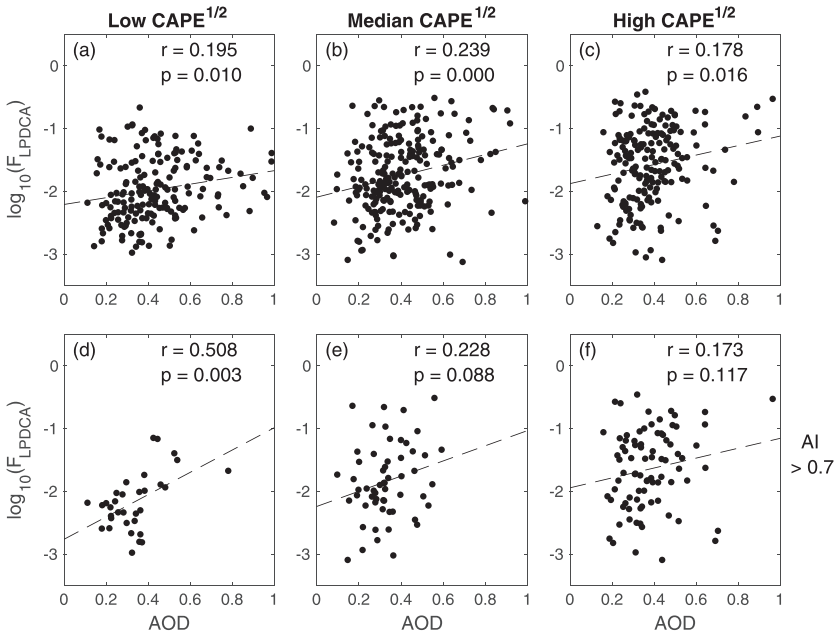

Figure 5. Scatterplots of $\log_{10}(F_{LPDCA})$ versus AOD in the low, median, and high $CAPE^{1/2}$ regimes, respectively, which are separated by a half standard deviation (σ_{CAPE}) below and above the mean (μ_{CAPE}) of the $CAPE^{1/2}$. $\mu_{CAPE} \pm \sigma_{CAPE}/2 = 27.51 \pm 9.92/2$ m·s^{-1} for all the storm cases (upper panels) and $27.56 \pm 10.03/2$ m·s^{-1} for all the cases where AI retrievals are available (lower panels). r and p in each panel are the correlation coefficient and the *p* value, respectively.

Niño–Southern Oscillation phases (Phillips et al., 1998; Ropelewski & Halpert, 1996). Figure 5 shows the scatterplots of $\log_{10}(F_{LPDCA})$ versus AOD in the low, median, and high $CAPE^{1/2}$ regimes, respectively. A bin plot of Figure 5 is provided in the supporting information (Figure S4).

The optical depth of all aerosols and storm area do not show significant correlations in the low and high CAPE regimes but a weak positive one with a *p* value smaller than 0.001 in the median CAPE regime (Figures 5a–5c). This result again suggests little overall influence of aerosols on lightning. The optical depth of absorbing aerosols and storm area shows a moderate correlation in the low $CAPE^{1/2}$ regime (Figure 5d)

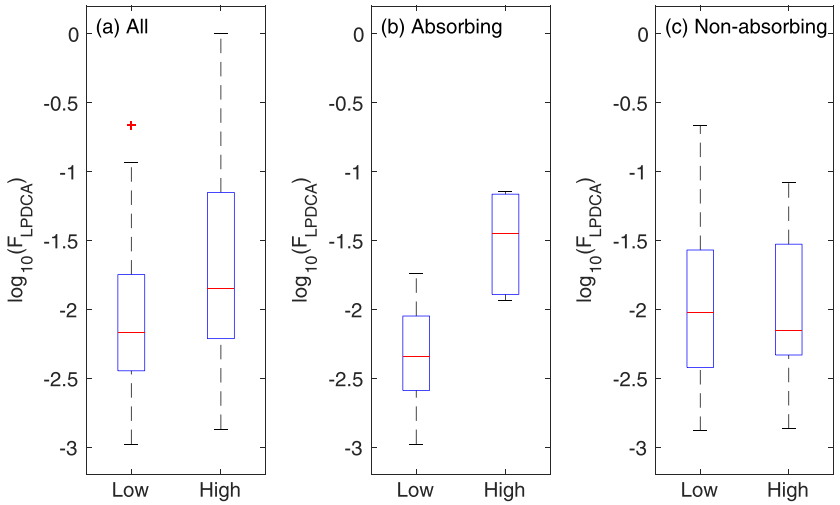

Figure 6. Boxplots of $\log_{10}(F_{LPDCA})$ in the intervals $0.2 \le AOD < 0.4$ (low) and $0.4 \le AOD < 0.6$ (high) for all cases (a), absorbing aerosol cases (b), and nonabsorbing aerosol cases (c) in the low $CAPE^{1/2}$ regime, respectively. In each panel, the central red lines are the medians. The bottom and top edges of the blue boxes are the 25th and 75th percentiles, respectively. The whiskers extend to the most extreme samples with the outliers (red plus) excluded.

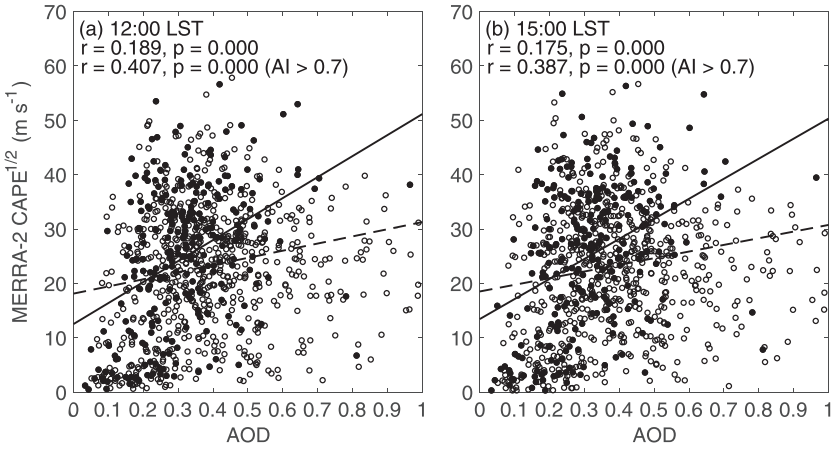

Figure 7. Scatterplots of the MERRA-2 $CAPE^{1/2}$ at 12:00 LST versus AOD (a) and the MERRA-2 $CAPE^{1/2}$ at 15:00 LST versus AOD (b) during the JJAs from 2002 to 2015. Among the cases from 2005 to 2015, those AIs greater than 0.7 are marked by dots. In each panel, the dashed line is the linear regression of $CAPE^{1/2}$ on AOD for all the cases (dots and circles) irrespective of their AIs; the upper r and p are the corresponding correlation coefficient and *p* value, respectively. The solid line is the linear regression of $CAPE^{1/2}$ on AOD for all the cases from 2005 to 2015 where AIs are greater than 0.7 (dots); the lower r and p are the corresponding correlation coefficient and *p* value, respectively. The Aqua MODS AOD retrievals date back to 2002; the OMI AI retrievals date back to 2005.

with a correlation coefficient of 0.508 and a *p* value of 0.003. The correlation coefficient is greater than that (0.195) between the optical depth of all aerosols and the storm area (Figure 5a), as suggested by a *p* value of 0.034 from a one-sided *z* test. Relaxing the assumption of linear relationships between AOD and CAPE, in the low $CAPE^{1/2}$ regime, the difference between the means of $\log_{10}(F_{LPDCA})$ in the intervals $0.2 \leq AOD < 0.4$ and $0.4 \leq AOD < 0.6$ are statistically significant ($p < 0.001$) in the presence of absorbing aerosols using two sampled *t* testing (Figure S4). Figure 6 shows the boxplots of $\log_{10}(F_{LPDCA})$ in the intervals $0.2 \leq AOD < 0.4$ and $0.4 \leq AOD < 0.6$ in the low $CAPE^{1/2}$ regime. As previously mentioned, no prior studies have suggested that the CCN/IN mechanism works better for more absorbing aerosols. Hence, the radiative effect of aerosols presumably applies with the positive correlation between the loading of absorbing aerosols and the storm area in the low $CAPE^{1/2}$ regime (Figures 5a and 5d). Perhaps, convection is more readily triggered in the environment conductive to stronger storms—such as the frontal systems—in the

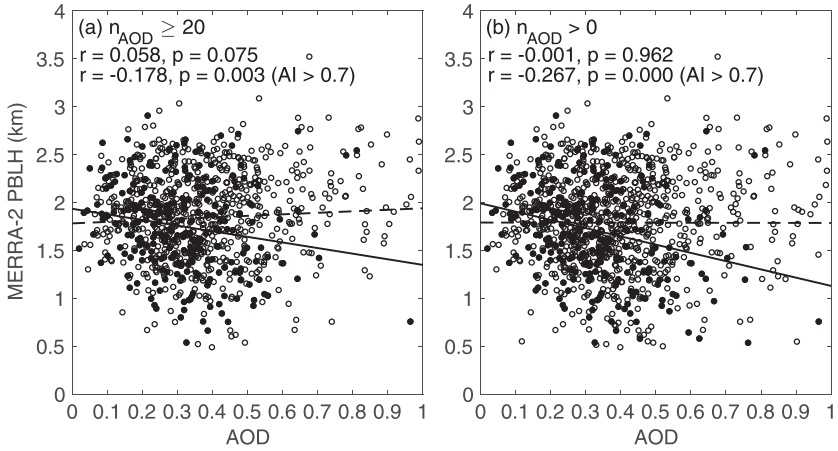

Figure 8. Scatterplots of PBLH versus AOD for the cases that have at least 20 available AOD retrievals (a) and all the cases (b) during the JJAs from 2002 to 2015. Among the cases from 2005 to 2015, those AIs greater than 0.7 are marked by dots. In each panel, the dashed line is the linear regression of PBLH on AOD for all the cases (dots and circles) irrespective of their AIs; the upper r and p are the corresponding correlation coefficient and *p* value, respectively. The solid line is the linear regression of PBLH on AOD for all the cases from 2005 to 2015 where AIs are greater than 0.7 (dots); the lower r and p are the corresponding correlation coefficient and *p* value, respectively. n_{AOD} is the number of the available AOD retrievals. The Aqua MODS AOD retrievals date back to 2002; the OMI AI retrievals date back to 2005.

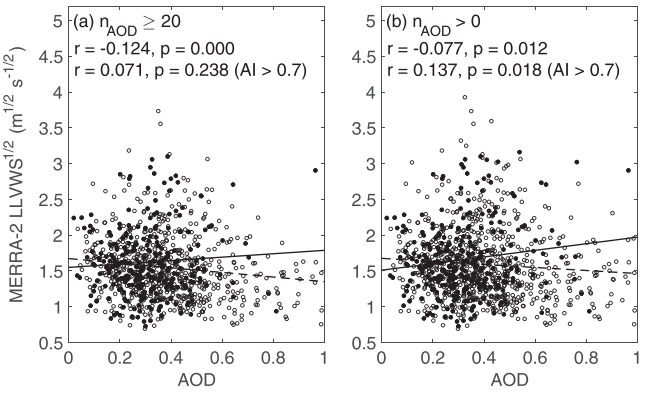

Figure 9. Same as Figure 8 except for the MERRA-2 LLVWS$^{1/2}$ versus AOD.

median and high CAPE regimes, making the warming of absorbing aerosols on top of the PBL less efficient in inhibiting convection. In the environment conductive to weaker storms in the low CAPE regime, the suppression of convection by absorbing aerosols is more efficient, leaving a longer CAPE accumulation period before convection is triggered. AOD and $\log_{10}$(FR/LPDCA) do not show any statistically significant linear correlations except a negative one in the median CAPE$^{1/2}$ regime in the presence of all aerosols, which passes the *t* test at a 95% confidence interval (not shown).

3.4. The CAPE and PBL Mechanisms

As previously shown, lightning flashes (FR) and the storm area (F_{LPDCA}) have weak positive correlations with the optical depth of absorbing aerosols, particularly in the low CAPE regime, leading to the speculation that the CAPE and PBL mechanisms apply in such storm cases. As shown in Figure 7, AOD is positively correlated with CAPE$^{1/2}$ during the active lightning period (15:00 LST) and before (12:00 LST) for all the storm cases. The correlation coefficients at 12:00 and 15:00 LST double for the cases in the presence of absorbing aerosols (Figure 7), significantly greater than the counterparts for all the storm cases with the one-sided *z* test *p* values smaller than 0.001 and 0.001, respectively. A bin plot of Figure 7 is provided in the supporting information (Figure S6). The difference between the means of CAPE$^{1/2}$ in the intervals $0.0 \leq \text{AOD} < 0.2$ and $0.4 \leq \text{AOD} < 0.6$ are statistically significant ($p < 0.001$) in the presence of both absorbing and nonabsorbing aerosols (Figure S6). The CAPE mechanism presumably applies with the positive correlation between CAPE and AOD in the presence of absorbing aerosols. The result is the same if the CAPE above 900 or 850 hPa is used instead of the surface CAPE (not shown). The significant difference in the CAPE$^{1/2}$ means between $0.0 \leq \text{AOD} < 0.2$ and $0.4 \leq \text{AOD} < 0.6$ for nonabsorbing aerosols suggests that there may be some unknown variable regulating CAPE and aerosols at the same time. As shown in Figure 8, AOD and the mean PBLH during the active lightning period show no correlations for all the storm cases but negative correlations for the cases in the presence of absorbing aerosols, given the correlations Ding et al. (2016) and Dong et al. (2017) found in their studies. The correlation is even more negative when all the storm cases that have at least one MODIS AOD retrieval within the study area are included (Figure 8b), that is, relaxing the spatial representativeness criterion. The correlation coefficients in the presence of absorbing aerosols are significantly smaller than those for all the storm cases with one-sided *z* test *p* values smaller than 0.001 (Figure 8a) and 0.001 (Figure 8b), respectively. A bin plot of Figure 8 is provided in the supporting information (Figure S8). The PBLH mean in the interval $0.0 \leq \text{AOD} < 0.2$ is significantly higher than that in $0.4 \leq \text{AOD} < 0.6$ ($p < 0.001$) in the presence of absorbing aerosols, when all the storm cases that have at least one MODIS AOD retrieval within the study area are included (Figure S8). However, the PBLH means do not show any significant differences in different AOD intervals in the presence of nonabsorbing aerosols (Figure S8). The optical depth of absorbing aerosols and the mean PBLH also show a negative correlation during 12:00–14:00 LST that falls within the timespan of the Aqua satellite overpass (not shown). While these negative correlations are suggestive, AOD and LLVWS do not show any significant linear relationships, regardless of the absorbance of aerosols (Figure 9). A bin plot of Figure 9 is provided in the supporting information (Figure S10). None of the differences in LLVWS$^{1/2}$ means between the high AOD interval ($0.4 \leq \text{AOD} < 0.6$) and the low AOD interval ($0.0 \leq \text{AOD} < 0.2$ or $0.2 \leq \text{AOD} < 0.4$) is statistically significant, regardless of the absorbance of aerosols (Figure S10). Hence, though increased absorbing aerosols are associated with reduced PBLHs, it does not appear that increased absorbing aerosols are associated with any detectably enhanced LLVWSs in this study.

3.5. Case Studies

3.5.1. Selection of Two Cases

A polluted case and a clean case (Table 5) are subjectively selected to illustrate the lightning and associated convection features in more detail with a focus on the CCN/IN and PBL mechanisms using additional observations. Both the cases are taken from the low CAPE$^{1/2}$ regime, where the optical depth of absorbing

Table 5
The Lightning, Aerosol, and Meteorological Parameters of the Selected Two Cases

Date	$\log_{10}$ (FR)	$\log_{10}(F_{LPDCA})$ (≥30 dBZ)	$\log_{10}$(FR/LPDCA) (≥30 dBZ)	AI	AOD	$CAPE^{1/2}$ ($m{\cdot}s^{-1}$)
18 August 2012	0.923	−1.501	−2.503	12.5	0.54	12.5
4 August 2015	0.219	−2.188	−2.444	14.3	0.20	19.2

aerosols correlates best with $\log_{10}(F_{LPDCA})$ (Figure 5). Only those cases that have CALIPSO satellite overpasses and radar polarimetric measurements are considered in the selection for a more detailed analysis.

The AODs of the polluted (18 August 2012) and clean (4 August 2015) cases were 0.54 (95th percentile) and 0.20 (21st percentile), respectively. Although the mean FRs per storm area in the two cases were close, the polluted case showed a larger mean storm area than the clean case (Table 5). As a result, more lightning flashes were detected during the active lightning period in the polluted case than in the clean case (Table 5). The CAPE of the polluted case was smaller than that of the clean case (Table 5), but both were within the low $CAPE^{1/2}$ regime. The large AI (Table 5) in the two cases is suggestive of the presence of absorbing aerosols in both cases, which are also supported by the CALIOP aerosol type retrievals (Figure 10). In the early afternoon (13:10 LST) of 18 August 2012, a smoke layer was detected between 2 and 3 km near the southern boundary of the study area and a polluted dust layer was detected below 2 km near the center of the study area (Figure 10). In the early afternoon (13:04 LST) of 4 August 2015, polluted dust aerosols were detected below 2 km along the track of CALIOP in the eastern part of the study area and between 4 and 5 km near the northeastern boundary.

3.5.2. The CCN/IN Mechanism

In the polluted case, most lightning flashes were produced by a cluster of convective cells that formed in the southern part of the study area (Figure 11a). New cells formed and old cells decayed as this cluster moved eastward. In addition, a strong single cell that occurred close to the southeastern edge of the study area also produced a portion of the flashes (Figure 11a). The convective area extended to Mississippi along a stationary front (Figure 11a). In the clean case, the lightning flashes were contributed by a few single cells; no multicell convective system was present. The polluted case shows a maximum FR of 17.00 min^{-1} during the radar scan that started at 15:03 LST (Figure 11a). The clean case shows a maximum FR of 8.00 min^{-1} during

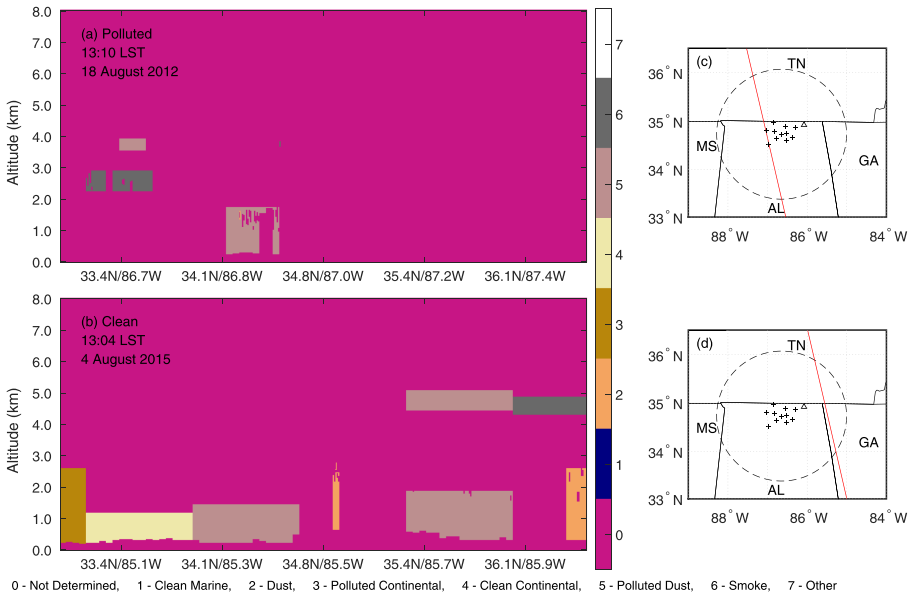

Figure 10. Vertical profiles of aerosol types along the tracks of CALIOP over the study area for the two selected cases, 18 August 2012 (a) and 4 August 2015 (c), respectively. The red lines in panels (c) and (d) mark the ground tracks of CALIOP on the map.

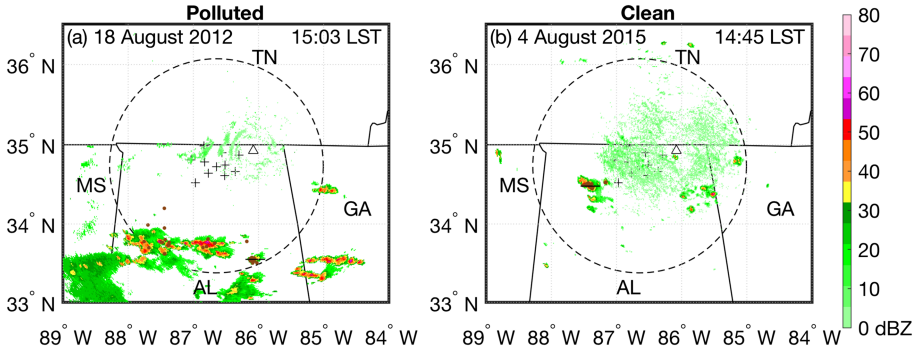

Figure 11. Spatial distributions of composite radar reflectivity when FR peaked during the active lightning period in the polluted (a) and clean (b) cases. In each panel, the horizontal black line across the convective cell marks the location where the vertical cross sections of Z (Figure 12) and Z_{DR} (Figure 13) are shown. AL, GA, MS, and TN are short for Alabama, Georgia, Mississippi, and Tennessee, respectively. The pluses are the detector locations of the NALMA. There were 10 NALMA stations before 2008, 11 in 2008, and 14 after 2008. The pluses in each panel mark the locations of the 11 NALMA stations through 2008. Not shown are three stations, one in Tennessee and two in Georgia, built after 2008. The triangle is the location of the KHTX site.

the radar scan that started at 14:45 LST (Figure 11b). The development of individual cells (Figure 11) in the polluted and clean cases is shown by their vertical cross sections of Z (Figure 12) and Z_{DR} (Figure 13) from five consecutive radar scans right before their peak FRs.

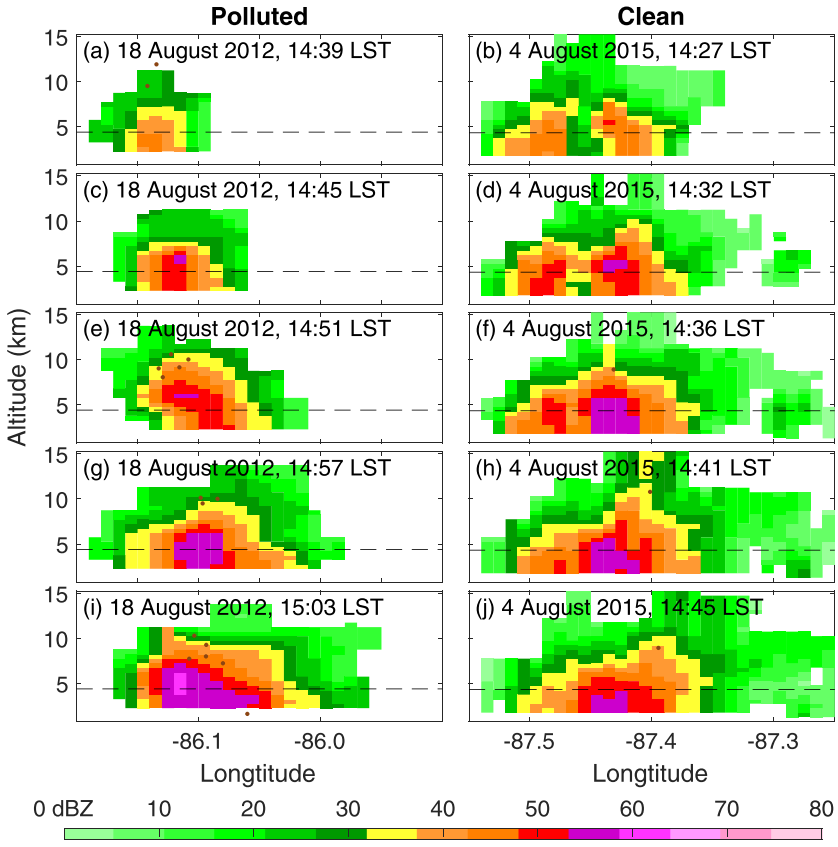

Figure 12. Vertical cross sections of Z (dBZ) at five consecutive radar scans for the two selected cases. The left and right panels are for the polluted and clean cases, respectively. In each panel, brown dots are the detected lightning flashes; the dashed black line is the freezing level taken from the MERRA-2.

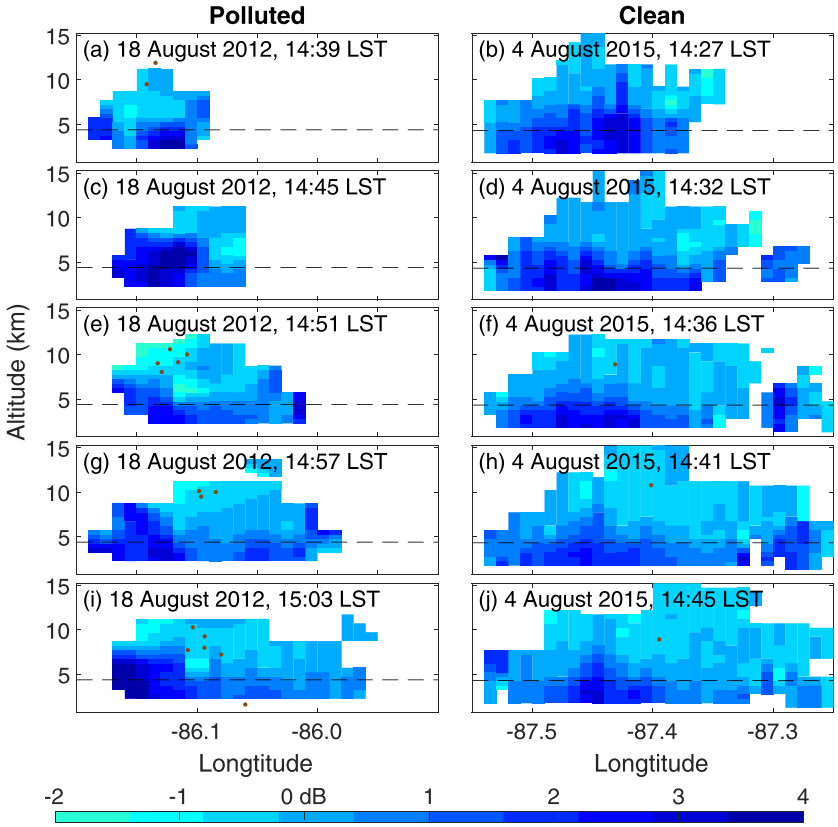

Figure 13. Same as Figure 12 except for Z_{DR} (dB).

The Z maxima above the freezing levels were close in the two cases (Figures 12a–12h) before their peak FRs. The Z maximum above the freezing level at the mature stage of the convective cell was greater in the polluted case (Figure 12i) than the counterpart in the clean case (Figure 12j), suggestive of a more invigorated convective cell with more supercooled water lifted above the freezing level in the polluted case (Yuan et al., 2011; Zipser & Lutz, 1994). A column of enhanced Z_{DR} around 4.0 was present above the freezing level at 14:45 LST in the polluted case (Figure 13c), suggesting the presence of increased supercooled water (Bruning et al., 2007; Conway & Zrnić, 1993; Herzegh & Jameson, 1992; Hubbert et al., 1998; Tuttle et al., 1989) at the growing stage of the convective cell right before the initialization of lightning flashes (Figure 13e). In agreement with a previous study by Bruning et al. (2007), the enhanced Z_{DR} column collapsed right before the initialization of the lightning flashes (Figure 13e), indicative of large ice formation near the lightning initialization locations.

Although increased supercooled water was evidently present above the freezing level in the polluted case based on the single cell comparison, this feature did not necessarily suggest that the CCN/IN mechanism applied to the polluted case. First, we cannot show that the convective cell in the polluted case had an increased number concentration of smaller cloud droplets at the developing stage of convection. The cloud droplet number concentration is dependent upon updraft velocity and aerosol particle number concentration (Ghan et al., 1993; Reutter et al., 2009; Twomey, 1959). We did not show the updraft velocities of the two cases, which were difficult to estimate. Moreover, the synoptic-scale environments of the two cases were different. A stationary front was formed in the polluted case from central Texas to central Mississippi at 08:00 LST and last 9 hr until the warm front triumphed over the cold front at 17:00 LST. The occurrence of the thunderstorms during the active lightning period over northern Alabama appeared to be influenced by this stationary front. However, in the clean case, no synoptic-scale weather system was present over the study area or nearby; the occurrence of the thunderstorms appeared to be local thermally driven. Therefore, in spite of the close CAPEs in the two selected cases, other possible factors that could affect the cloud

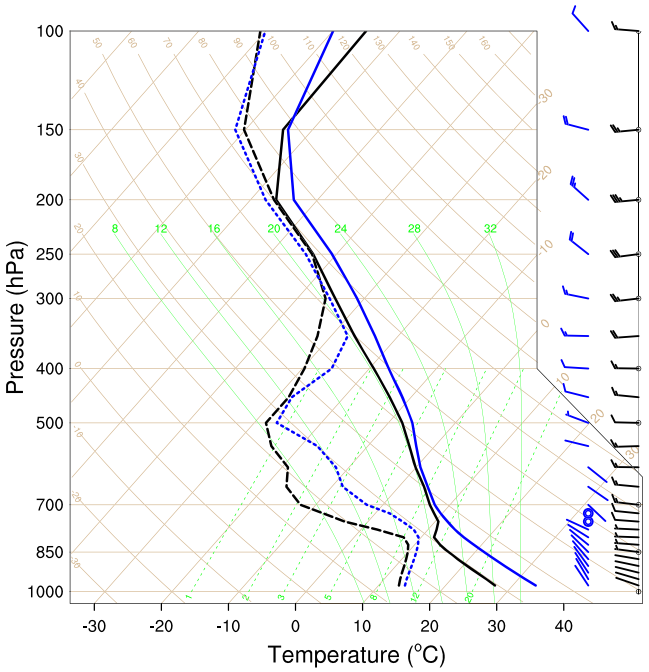

Figure 14. Skew-T log-P diagram at 15:00 LST for the two selected cases. The black solid and dashed curves are the vertical profiles of domain-averaged MERRA-2 temperature and dew point temperature of the polluted case (18 August 2012), respectively. The blue ones are of the clean case (4 August 2015). The black and blue wind barbs are the vertical profiles of domain-averaged MERRA-2 horizontal winds of the polluted and clean cases, respectively.

microphysics might not be ruled out. Recent studies (Rosenfeld et al., 2014; Rosenfeld et al., 2016; Zheng et al., 2015) have suggested a way of estimating CCN concentrations and cloud base updraft velocities of boundary layer convective clouds simultaneously using satellite observations. Such satellite retrievals, if available, may help disentangle the CCN/IN mechanism from the influences on deep convection by other factors.

3.5.3. The PBL Mechanism

The vertical thermal structures of the two cases were different. A heated layer between 850 and 700 hPa was present at 15:00 LST before the active lightning period in the polluted case, as shown by the reduced lapse rate in this layer (Figure 14). The surface temperature was cooler in the polluted case than in the clean case. The cooling of the surface and heating aloft in the polluted case were presumably contributed by the absorbing aerosol layer between 2 and 3 km (Figure 10a) and/or the passage of a cold front at least 8 hr ago (not shown). The LLVWS (below 700 hPa) at 15:00 LST was stronger in the polluted case than in the clean case (Figure 14). The result was the same at 12:00 LST (not shown). However, the stronger low-level wind shear in the polluted case might also be due to the eastward propagation of the storms that occurred over the study area, not far from a stationary front in Mississippi. Hence, other factors that may lead to enhanced wind shear could not be excluded.

4. Discussion and Conclusions

Recent studies have suggested simultaneous influences of normalized CAPE and aerosols on deep convection and lightning over the tropics (Stolz et al., 2015; Stolz et al., 2017). By contrast, the lightning FR during the diurnal-peak period (14:00–17:00 LST) and satellite AOD retrievals in the early afternoon over northern Alabama generally do not show any significant linear relationships. This result, in the context of ensembles of deep convective clouds, calls the convection invigoration process that is suggested in the context of a single cloud (e.g., Rosenfeld et al., 2008) into question. In agreement with some modeling results (e.g., Grabowski, 2015; Grabowski & Morrison, 2016), the lack of a correlation between AOD and FR in this study highlights the necessity of a dichotomy of the process-level reasoning versus the system dynamic reasoning (Grabowski, 2006). In other words, changes during a period in a part of a convective system may be compensated for by an opposite change when the entire system is treated as a whole (Grabowski, 2006; Grabowski & Morrison, 2011; Stevens & Feingold, 2009) and consequently such changes, if present, are extremely difficult to detect using the observations of the entire system (Stevens & Feingold, 2009). However, AOD and FR show a weak positive correlation in the presence of absorbing aerosols over northern Alabama, which appears to be contributed by the association between the abundance of absorbing aerosols and storm area, particularly in the low CAPE regime, leading us to speculate that the radiative effect of aerosols may play a role in regulating the storm intensity.

Absorbing aerosols on top of the PBL can suppress convection and lead to the accumulation of CAPE, resulting in more intense storms later when convection is triggered (Wang et al., 2013). This CAPE mechanism presumably applies with the positive correlation between AOD and CAPE in the presence of absorbing aerosols and hence is presumably a link between absorbing aerosols and lightning-producing storms. Moreover, the correlation between absorbing aerosols and storm area is strongest in the low CAPE regime. Convection is often triggered over the strong convergence zone of a cyclonic system, where the warming layer of absorbing aerosols aloft is presumably not strong enough to inhibit the convection. However, the warming layer of absorbing aerosols may be more efficient in suppressing the local thermally driven convection, allowing a longer duration of CAPE accumulation before the convection is triggered. In addition, Saide et al. (2015) suggest that the suppression of the turbulent mixing within the PBL by absorbing aerosols may result in enhanced LLVWSs, which may in turn affect convection. However, in this study, although AOD and

PBLH show a negative correlation in the presence of absorbing aerosols, AOD and LLVWS do not show any significant linear relationships.

While the results may be suggestive of the CAPE mechanism, the correlation analysis based on observational data cannot exclude other factors that may result in the same correlation. In addition, as shown in the case studies in section 3.5, although it is possible to compare the strength of deep convection on a single cell basis using radar observations, it is extremely difficult to disentangle the aerosol impact on the convection invigoration process based on such observations, because it is nearly impossible to find two convective cells whose environments are convincingly close except the CCN concentrations. In addition, the CAPE and PBL mechanisms discussed in the study are caused by the local radiative effects of absorbing aerosols. However, numerous studies have shown that both anthropogenic and natural emissions of absorbing aerosols can interact with mesoscale and large-scale circulations with resultant redistributions of precipitation (e.g., Jin et al., 2015; Lau et al., 2008; Zhao et al., 2012). Whether the variation of FR over Northern Alabama is affected by the large-scale impact of absorbing aerosols is not addressed here. Moreover, AOD is a more commonly used metric for the radiative effects than for the microphysical effects of aerosols (Andreae, 2009). Absorbing aerosols—such as dust and smoke particles—are often less hygroscopic (Kim et al., 2006), and hence, variations in the optical depth of such absorbing aerosols and the CCN concentration may not be consistent. The correlations between aerosols and FR might be supportive of the CCN/IN mechanism, if CCN concentration were the measured quantity rather than AOD. Furthermore, the aerosol loading was characterized in a spatially averaged sense in this study, that is, averaging the AOD retrievals over the study area. However, aerosol impacts on convection are dependent upon the zones of a storm (Lin et al., 2016). Lin et al. (2016) suggest different responses of shallow cumuli and stratus to increased CCN, if the radiative effect of aerosols is also considered. Whether and how the spatial variability of aerosol loadings may influence a storm remains an area for further research.

Acknowledgments
We thank the Texas A&M High Performance Research Computing for providing the disk quota and software for processing the data in this work. Where the data supporting the conclusions of this study were accessed can be found in the references. We thank three anonymous reviewers for their helpful comments for this paper. A. D. Rapp and T. Ren's contributions were supported by NSF Grant AGS-1261392 at Texas A&M University; J. R. Mecikalski and J. Apke's contributions were supported by NSF Grant AGS-1261368. T. Ren appreciated his discussions with Dr. Souichiro Hioki, Dr. R. Bradley Pierce, and Dr. Gang Zhang about this study. The NALMA data were acquired from the Global Hydrology Resource Center (GHRC) Distributed Active Archive Center (DAAC), located in the National Space Science and Technology Center (NSSTC) in Huntsville, Alabama (https://ghrc.nsstc.nasa.gov/). The *Aqua* MODIS Aerosol 5-Min L2 Swath 3km V006 data sets were acquired from the Level-1 and Atmosphere Archive and Distribution System (LAADS) DAAC, located in the NASA Goddard Space Flight Center (GSFC) in Greenbelt, Maryland (https://ladsweb.nascom.nasa.gov/). The version 003 OMI Level 2 OMTO3 data sets were acquired from the Data and Information Services Center (DISC), located in the NASA GSFC in Greenbelt, Maryland (https://disc.gsfc.nasa.gov/). The MERRA-2 data were acquired from the Global Modeling and Assimilation Office (GMAO), located in the NASA GSFC in Greenbelt, Maryland (https://gmao.gsfc.nasa.gov/). The version 3.30 CALIOP Level 2 vertical feature mask data were acquired from the Atmospheric Science Data Center (ASDC), located in the NASA Langley Research Center in Hampton, Virginia (https://eosweb.larc.nasa.gov/). The WSR-88D radar data were acquired from the NOAA National Centers for Environmental Information (NCEI; https://www.ncdc.noaa.gov/).

References

Albrecht, B. A. (1989). Aerosols, cloud microphysics, and fractional cloudiness. *Science*, *245*(4923), 1227–1230. https://doi.org/10.1126/science.245.4923.1227

Albrecht, R. I., Goodman, S. J., Buechler, D. E., Blakeslee, R. J., & Christian, H. J. (2016). Where are the lightning hotspots on Earth? *Bulletin of the American Meteorological Society*, *97*(11), 2051–2068. https://doi.org/10.1175/BAMS-D-14-00193.2

Albrecht, R. I., Morales, C. A., & Silva Dias, M. A. (2011). Electrification of precipitating systems over the Amazon: Physical processes of thunderstorm development. *Journal of Geophysical Research*, *116*, D08209. https://doi.org/10.1029/2010JD014756

Altaratz, O., Koren, I., Remer, L., & Hirsch, E. (2014). Cloud invigoration by aerosols—Coupling between microphysics and dynamics. *Atmospheric Research*, *140*, 38–60. https://doi.org/10.1016/j.atmosres.2014.01.009

Altaratz, O., Koren, I., Yair, Y., & Price, C. (2010). Lightning response to smoke from Amazonian fires. *Geophysical Research Letters*, *37*, L07801. https://doi.org/10.1029/2010GL042679

Altaratz, O., Kucienska, B., Kostinski, A., Raga, G. B., & Koren, I. (2017). Global association of aerosol with flash density of intense lightning. *Environmental Research Letters*, *12*(11), 114037. https://doi.org/10.1088/1748-9326/aa922b

Andreae, M. O. (2009). Correlation between cloud condensation nuclei concentration and aerosol optical thickness in remote and polluted regions. *Atmospheric Chemistry and Physics*, *9*(2), 543–556. https://doi.org/10.5194/acp-9-543-2009

Andreae, M. O., Rosenfeld, D., Artaxo, P., Costa, A. A., Frank, G. P., Longo, K. M., & Silva-Dias, M. A. F. (2004). Smoking rain clouds over the Amazon. *Science*, *303*(5662), 1337–1342. https://doi.org/10.1126/science.1092779

Bhartia, P. K. (2005). OMI/Aura Ozone (O3) Total Column 1-Orbit L2 Swath 13x24 km V003, Greenbelt, MD, USA, Goddard Earth Sciences Data and Information Services Center (GES DISC), Accessed 25 September 2016, https://doi.org/10.5067/Aura/OMI/DATA 2024.

Blakeslee, R. J., Mach, D. M., Bateman, M. G., & Bailey, J. C. (2014). Seasonal variations in the lightning diurnal cycle and implications for the global electric circuit. *Atmospheric Research*, *135*, 228–243. https://doi.org/10.1016/j.atmosres.2012.09.023

Boccippio, D. J., Cummins, K. L., Christian, H. J., & Goodman, S. J. (2001). Combined satellite-and surface-based estimation of the intracloud–cloud-to-ground lightning ratio over the continental United States. *Monthly Weather Review*, *129*(1), 108–122. https://doi.org/10.1175/1520-0493(2001)129<0108:CSASBE>2.0.CO;2

Bringi, V., Knupp, K., Detwiler, A., Liu, L., Caylor, I., & Black, R. (1997). Evolution of a Florida thunderstorm during the Convection and Precipitation/Electrification experiment: The case of 9 August 1991. *Monthly Weather Review*, *125*(9), 2131–2160. https://doi.org/10.1175/1520-0493(1997)125<2131:EOAFTD>2.0.CO;2

Bruning, E. C., Rust, W. D., Schuur, T. J., MacGorman, D. R., Krehbiel, P. R., & Rison, W. (2007). Electrical and polarimetric radar observations of a multicell storm in TELEX. *Monthly Weather Review*, *135*(7), 2525–2544. https://doi.org/10.1175/MWR3421.1

Byers, H. R., & Braham, R. R. (1949). *The thunderstorm: Report of the Thunderstorm Project*. Washington, DC: US Government Printing Office.

CALIPSO Science Team (2015). CALIPSO/CALIOP Level 2, Vertical Feature Mask Data, version 3.30, Hampton, VA, USA: NASA Atmospheric Science Data Center (ASDC), Accessed 3 May 2016 at doi: 10.5067/CALIOP/CALIPSO/CAL_LID_L2_VFM-ValStage1-V3-30_L2-003.30

Carey, L., & Rutledge, S. (1996). A multiparameter radar case study of the microphysical and kinematic evolution of a lightning producing storm. *Meteorology and Atmospheric Physics*, *59*(1-2), 33–64. https://doi.org/10.1007/BF01032000

Carey, L., & Stough, S. (2016). North Alabama Lightning Mapping Array (NALMA) Data. Version 1.0. UCAR/NCAR—Earth Observing Laboratory. https://doi.org/10.5065/D6Z899T8. .

Carey, L. D., & Rutledge, S. A. (2000). The relationship between precipitation and lightning in tropical island convection: A C-band polarimetric radar study. *Monthly Weather Review*, *128*(8), 2687–2710. https://doi.org/10.1175/1520-0493(2000)128<2687:TRBPAL>2.0.CO;2

Chiapello, I., & Moulin, C. (2002). TOMS and METEOSAT satellite records of the variability of Saharan dust transport over the Atlantic during the last two decades (1979–1997). *Geophysical Research Letters*, *29*(8), 1176. https://doi.org/10.1029/2001GL013767

Chmielewski, V. C., & Bruning, E. C. (2016). Lightning mapping array flash detection performance with variable receiver thresholds. *Journal of Geophysical Research: Atmospheres*, *121*, 8600–8614. https://doi.org/10.1002/2016JD025159

Christian, H. J., Blakeslee, R. J., Boccippio, D. J., Boeck, W. L., Buechler, D. E., Driscoll, K. T., et al. (2003). Global frequency and distribution of lightning as observed from space by the optical transient detector. *Journal of Geophysical Research*, *108*(D1), 4005. https://doi.org/10.1029/2002JD002347

Chronis, T., & Koshak, W. J. (2016). Diurnal variation of TRMM/LIS lightning flash radiances. *Bulletin of the American Meteorological Society*. https://doi.org/10.1175/BAMS-D-16-0041.1

Conway, J. W., & Zrnić, D. S. (1993). A study of embryo production and hail growth using dual-Doppler and multiparameter radars. *Monthly Weather Review*, *121*(9), 2511–2528. https://doi.org/10.1175/1520-0493(1993)121<2511:ASOEPA>2.0.CO;2

Coquillat, S., Boussaton, M.-P., Buguet, M., Lambert, D., Ribaud, J.-F., & Berthelot, A. (2013). Lightning ground flash patterns over Paris area between 1992 and 2003: Influence of pollution? *Atmospheric Research*, *122*, 77–92. https://doi.org/10.1016/j.atmosres.2012.10.032

Cziczo, D., Murphy, D., Hudson, P., & Thomson, D. (2004). Single particle measurements of the chemical composition of cirrus ice residue during CRYSTAL–FACE. *Journal of Geophysical Research*, *109*, D04201. https://doi.org/10.1029/2003JD004032

Deierling, W., & Petersen, W. A. (2008). Total lightning activity as an indicator of updraft characteristics. *Journal of Geophysical Research*, *113*, D16210. https://doi.org/10.1029/2007JD009598

Deierling, W., Petersen, W. A., Latham, J., Ellis, S., & Christian, H. J. (2008). The relationship between lightning activity and ice fluxes in thunderstorms. *Journal of Geophysical Research*, *113*, D15210. https://doi.org/10.1029/2007JD009700

DeMott, P., Cziczo, D., Prenni, A., Murphy, D., Kreidenweis, S., Thomson, D., et al. (2003). Measurements of the concentration and composition of nuclei for cirrus formation. *Proceedings of the National Academy of Sciences*, *100*(25), 14,655–14,660. https://doi.org/10.1073/pnas.2532677100

DeMott, P. J., Sassen, K., Poellot, M. R., Baumgardner, D., Rogers, D. C., Brooks, S. D., et al. (2003). African dust aerosols as atmospheric ice nuclei. *Geophysical Research Letters*, *30*(14), 1732. https://doi.org/10.1029/2003GL017410

Ding, A., Huang, X., Nie, W., Sun, J., Kerminen, V. M., Petäjä, T., et al. (2016). Enhanced haze pollution by black carbon in megacities in China. *Geophysical Research Letters*, *43*, 2873–2879. https://doi.org/10.1002/2016GL067745

Dong, Z., Li, Z., Yu, X., Cribb, M., Li, X., & Dai, J. (2017). Opposite long-term trends in aerosols between low and high altitudes: a testimony to the aerosol–PBL feedback. *Atmospheric Chemistry and Physics*, *17*(12), 7997–8009. https://doi.org/10.5194/acp-17-7997-2017

Dye, J., Jones, J., Winn, W., Cerni, T., Gardiner, B., Lamb, D., et al. (1986). Early electrification and precipitation development in a small, isolated Montana cumulonimbus. *Journal of Geophysical Research*, *91*(D1), 1231–1247. https://doi.org/10.1029/JD091iD01p01231

Emanuel, K. A. (1994). *Atmospheric convection*. New York: Oxford University Press.

Fan, J., Yuan, T., Comstock, J. M., Ghan, S., Khain, A., Leung, L. R., et al. (2009). Dominant role by vertical wind shear in regulating aerosol effects on deep convective clouds. *Journal of Geophysical Research*, *114*, D22206. https://doi.org/10.1029/2009JD012352

Fan, J., Zhang, R., Tao, W. K., & Mohr, K. I. (2008). Effects of aerosol optical properties on deep convective clouds and radiative forcing. *Journal of Geophysical Research*, *113*, D08209. https://doi.org/10.1029/2007JD009257

Feingold, G. (2003). First measurements of the Twomey indirect effect using ground-based remote sensors. *Geophysical Research Letters*, *30*(6), 1287. https://doi.org/10.1029/2002GL016633

Fernandes, W. A., Pinto, I. R., Pinto, O. Jr., Longo, K. M., & Freitas, S. R. (2006). New findings about the influence of smoke from fires on the cloud-to-ground lightning characteristics in the Amazon region. *Geophysical Research Letters*, *33*, L20810. https://doi.org/10.1029/2006GL027744

Flannigan, M., & Wotton, B. (1991). Lightning-ignited forest fires in northwestern Ontario. *Canadian Journal of Forest Research*, *21*(3), 277–287. https://doi.org/10.1139/x91-035

Ghan, S. J., Chung, C. C., & Penner, J. E. (1993). A parameterization of cloud droplet nucleation part I: single aerosol type. *Atmospheric Research*, *30*(4), 198–221. https://doi.org/10.1016/0169-8095(93)90024-I

Global Modeling and Assimilation Office (GMAO). (2015a). MERRA-2 inst3_3d_asm_Np: 3d, 3-Hourly,Instantaneous,Pressure-Level, Assimilation,Assimilated Meteorological Fields V5.12.4. Goddard Earth Sciences Data and Information Services Center (GES DISC), accessed 7 August 2017, https://doi.org/10.5067/QBZ6MG944HW0

Global Modeling and Assimilation Office (GMAO). (2015b). MERRA-2 inst3_3d_asm_Nv: 3d, 3-Hourly,Instantaneous,Model-Level, Assimilation,Assimilated Meteorological Fields V5.12.4. Goddard Earth Sciences Data and Information Services Center (GES DISC), accessed 16 February 2017, https://doi.org/10.5067/WWQSXQ8IVFW8

Global Modeling and Assimilation Office (GMAO). (2015c). MERRA-2 tavg1_2d_flx_Nx: 2d,1-Hourly,Time-Averaged,Single-Level, Assimilation,Surface Flux Diagnostics V5.12.4. Goddard Earth Sciences Data and Information Services Center (GES DISC), accessed 29 November 2016, https://doi.org/10.5067/7MCPBJ41Y0K6

Global Modeling and Assimilation Office (GMAO). (2015d). MERRA-2 tavg1_2d_slv_Nx: 2d,1-Hourly,Time-Averaged,Single-Level, Assimilation,Single-Level Diagnostics V5.12.4. Goddard Earth Sciences Data and Information Services Center (GES DISC), accessed 29 November 2016 and 8 September 2018, https://doi.org/10.5067/VJAFPLI1CSIV

Goodman, S., Blakeslee, R., Christian, H., Koshak, W., Bailey, J., Hall, J., et al. (2005). The North Alabama lightning mapping array: Recent severe storm observations and future prospects. *Atmospheric Research*, *76*(1-4), 423–437. https://doi.org/10.1016/j.atmosres.2004.11.035

Goodman, S. J., Buechler, D. E., Wright, P. D., & Rust, W. D. (1988). Lightning and precipitation history of a microburst–producing storm. *Geophysical Research Letters*, *15*(11), 1185–1188. https://doi.org/10.1029/GL015i011p01185

Grabowski, W. W. (2006). Indirect impact of atmospheric aerosols in idealized simulations of convective–radiative quasi equilibrium. *Journal of Climate*, *19*(18), 4664–4682. https://doi.org/10.1175/JCLI3857.1

Grabowski, W. W. (2015). Untangling microphysical impacts on deep convection applying a novel modeling methodology. *Journal of the Atmospheric Sciences*, *72*(6), 2446–2464. https://doi.org/10.1175/JAS-D-14-0307.1

Grabowski, W. W., & Morrison, H. (2011). Indirect impact of atmospheric aerosols in idealized simulations of convective–radiative quasi equilibrium. Part II: Double-moment microphysics. *Journal of Climate*, *24*(7), 1897–1912. https://doi.org/10.1175/2010JCLI3647.1

Grabowski, W. W., & Morrison, H. (2016). Untangling microphysical impacts on deep convection applying a novel modeling methodology. Part II: Double-moment microphysics. *Journal of the Atmospheric Sciences*, *73*(9), 3749–3770. https://doi.org/10.1175/JAS-D-15-0367.1

He, Q., Li, C., Mao, J., Lau, A. K.-H., & Chu, D. A. (2008). Analysis of aerosol vertical distribution and variability in Hong Kong. *Journal of Geophysical Research*, *113*, D14211. https://doi.org/10.1029/2008JD009778

Herman, J. R., Bhartia, P. K., Torres, O., Hsu, C., Seftor, C., & Celarier, E. (1997). Global distribution of UV-absorbing aerosols from Nimbus 7/TOMS data. *Journal of Geophysical Research*, *102*, 16,911–16,922. https://doi.org/10.1029/96JD03680

Herman, J., Krotkov, N., Celarier, E., Larko, D., & Labow, G. (1999). Distribution of UV radiation at the Earth's surface from TOMS-measured UV-backscattered radiances. *Journal of Geophysical Research*, *104*(D10), 12,059–12,076. https://doi.org/10.1029/1999JD900062

Herzegh, P. H., & Jameson, A. R. (1992). Observing precipitation through dual-polarization radar measurements. *Bulletin of the American Meteorological Society*, *73*(9), 1365–1374. https://doi.org/10.1175/1520-0477(1992)073<1365:OPTDPR>2.0.CO;2

Hoose, C., & Möhler, O. (2012). Heterogeneous ice nucleation on atmospheric aerosols: a review of results from laboratory experiments. *Atmospheric Chemistry and Physics*, *12*(20), 9817. https://doi.org/10.5194/acp-12-9817-2012

Hsu, N. C., Herman, J. R., Gleason, J., Torres, O., & Seftor, C. (1999). Satellite detection of smoke aerosols over a snow/ice surface by TOMS. *Geophysical Research Letters*, *26*(8), 1165–1168. https://doi.org/10.1029/1999GL900155

Hsu, N. C., Herman, J. R., & Tsay, S. C. (2003). Radiative impacts from biomass burning in the presence of clouds during boreal spring in southeast Asia. *Geophysical Research Letters*, *30*(5), 1224. https://doi.org/10.1029/2002GL016485

Huang, J., Fu, Q., Su, J., Tang, Q., Minnis, P., Hu, Y., et al. (2009). Taklimakan dust aerosol radiative heating derived from CALIPSO observations using the Fu-Liou radiation model with CERES constraints. *Atmospheric Chemistry and Physics*, *9*(12), 4011–4021. https://doi.org/10.5194/acp-9-4011-2009

Hubbert, J., Bringi, V., Carey, L., & Bolen, S. (1998). CSU-CHILL polarimetric radar measurements from a severe hail storm in eastern Colorado. *Journal of Applied Meteorology*, *37*(8), 749–775. https://doi.org/10.1175/1520-0450(1998)037<0749:CCPRMF>2.0.CO;2

Jaeglé, L. (2007). Pumping up surface air. *Science*, *315*(5813), 772–773. https://doi.org/10.1126/science.1138988

Jenkins, G. S., Pratt, A. S., & Heymsfield, A. (2008). Possible linkages between Saharan dust and tropical cyclone rain band invigoration in the eastern Atlantic during NAMMA–06. *Geophysical Research Letters*, *35*, L08815. https://doi.org/10.1029/2008GL034072

Jin, Q., Wei, J., Yang, Z.-L., Pu, B., & Huang, J. (2015). Consistent response of Indian summer monsoon to Middle East dust in observations and simulations. *Atmospheric Chemistry and Physics*, *1680*, 7324. https://doi.org/10.5194/acp-15-9897-2015

Khain, A., Rosenfeld, D., & Pokrovsky, A. (2005). Aerosol impact on the dynamics and microphysics of deep convective clouds. *Quarterly Journal of the Royal Meteorological Society*, *131*(611), 2639–2663. https://doi.org/10.1256/qj.04.62

Kim, J., Lee, J., Lee, H. C., Higurashi, A., Takemura, T., & Song, C. H. (2007). Consistency of the aerosol type classification from satellite remote sensing during the Atmospheric Brown Cloud–East Asia Regional Experiment campaign. *Journal of Geophysical Research*, *112*, D22S33. https://doi.org/10.1029/2006JD008201

Kim, J., Yoon, S.-C., Jefferson, A., & Kim, S.-W. (2006). Aerosol hygroscopic properties during Asian dust, pollution, and biomass burning episodes at Gosan, Korea in April 2001. *Atmospheric Environment*, *40*(8), 1550–1560. https://doi.org/10.1016/j.atmosenv.2005.10.044

Knupp, K. R., & Cotton, W. R. (1982). An intense, quasi-steady thunderstorm over mountainous terrain. Part II: Doppler radar observations of the storm morphological structure. *Journal of the Atmospheric Sciences*, *39*(2), 343–358.

Koch, D., & Del Genio, A. (2010). Black carbon semi-direct effects on cloud cover: Review and synthesis. *Atmospheric Chemistry and Physics*, *10*(16), 7685–7696. https://doi.org/10.5194/acp-10-7685-2010

Konrad, C. E. (1997). Synoptic-scale features associated with warm season heavy rainfall over the interior southeastern United States. *Weather and Forecasting*, *12*(3), 557–571. https://doi.org/10.1175/1520-0434(1997)012<0557:SSFAWW>2.0.CO;2

Koren, I., Feingold, G., & Remer, L. A. (2010). The invigoration of deep convective clouds over the Atlantic: Aerosol effect, meteorology or retrieval artifact? *Atmospheric Chemistry and Physics*, *10*(18), 8855–8872. https://doi.org/10.5194/acp-10-8855-2010

Koren, I., Kaufman, Y. J., Rosenfeld, D., Remer, L. A., & Rudich, Y. (2005). Aerosol invigoration and restructuring of Atlantic convective clouds. *Geophysical Research Letters*, *32*, L14828. https://doi.org/10.1029/2005GL023187

Koshak, W., Solakiewicz, R., Blakeslee, R., Goodman, S., Christian, H., Hall, J., et al. (2004). North Alabama Lightning Mapping Array (LMA): VHF source retrieval algorithm and error analyses. *Journal of Atmospheric and Oceanic Technology*, *21*(4), 543–558. https://doi.org/10.1175/1520-0426(2004)021<0543:NALMAL>2.0.CO;2

Larsen, H., & Stansbury, E. (1974). Association of lightning flashes with precipitation cores extending to height 7 km. *Journal of Atmospheric and Terrestrial Physics*, *36*(9), 1547IN231549-15481553. https://doi.org/10.1016/0021-9169(74)90232-3

Lau, K., Tsay, S., Ramanathan, V., Wu, G.-X., Li, Z., Tsay, S. C., et al. (2008). The Joint Aerosol–Monsoon Experiment: A new challenge for monsoon climate research. *Bulletin of the American Meteorological Society*, *89*(3), 369–384. https://doi.org/10.1175/BAMS-89-3-369

Lee, S. S., & Feingold, G. (2010). Precipitating cloud–system response to aerosol perturbations. *Geophysical Research Letters*, *37*, L23806. https://doi.org/10.1029/2010GL045596

Levelt, P. F., van den Oord, G. H., Dobber, M. R., Malkki, A., Visser, H., de Vries, J., et al. (2006). The ozone monitoring instrument. *IEEE Transactions on Geoscience and Remote Sensing*, *44*(5), 1093–1101. https://doi.org/10.1109/TGRS.2006.872333

Levi, Y., & Rosenfeld, D. (1996). Ice nuclei, rainwater chemical composition, and static cloud seeding effects in Israel. *Journal of Applied Meteorology*, *35*(9), 1494–1501. https://doi.org/10.1175/1520-0450(1996)035<1494:INRCCA>2.0.CO;2

Levy, R., Hsu C., et al. (2015). MODIS Atmosphere L2 Aerosol Product. NASA MODIS Adaptive Processing System, Goddard Space Flight Center, USA: https://doi.org/10.5067/MODIS/MYD04_L2.006

Levy, R. C., Mattoo, S., Munchak, L. A., Remer, L. A., Sayer, A. M., Patadia, F., & Hsu, N. C. (2013). The Collection 6 MODIS aerosol products over land and ocean. *Atmospheric Measurement Techniques*, *6*(11), 2989–3034. https://doi.org/10.5194/amt-6-2989-2013

Levy, R. C., Remer, L. A., & Dubovik, O. (2007). Global aerosol optical properties and application to Moderate Resolution Imaging Spectroradiometer aerosol retrieval over land. *Journal of Geophysical Research*, *112*, D13210. https://doi.org/10.1029/2006JD007815

Levy, R. C., Remer, L. A., Mattoo, S., Vermote, E. F., & Kaufman, Y. J. (2007). Second–generation operational algorithm: Retrieval of aerosol properties over land from inversion of Moderate Resolution Imaging Spectroradiometer spectral reflectance. *Journal of Geophysical Research*, *112*, D13211. https://doi.org/10.1029/2006JD007811

Li, G., Wang, Y., & Zhang, R. (2008). Implementation of a two-moment bulk microphysics scheme to the WRF model to investigate aerosol-cloud interaction. *Journal of Geophysical Research*, *113*, D15211. https://doi.org/10.1029/2007JD009361

Li, Z., Guo, J., Ding, A., Liao, H., Liu, J., Sun, Y., et al. (2017). Aerosol and boundary-layer interactions and impact on air quality. *National Science Review*, *4*(6), 810–833. https://doi.org/10.1093/nsr/nwx117

Li, Z., Lee, K. H., Wang, Y., Xin, J., & Hao, W. M. (2010). First observation-based estimates of cloud-free aerosol radiative forcing across China. *Journal of Geophysical Research*, *115*, D00K18. https://doi.org/10.1029/2009JD013306

Li, Z., Xue, H., & Yang, F. (2013). A modeling study of ice formation affected by aerosols. *Journal of Geophysical Research: Atmospheres*, *118*, 11,213–11,227. https://doi.org/10.1002/jgrd.50861

Lin, Y., Wang, Y., Pan, B., Hu, J., Liu, Y., & Zhang, R. (2016). Distinct impacts of aerosols on an evolving continental cloud complex during the RACORO field campaign. *Journal of the Atmospheric Sciences*, *73*(9). https://doi.org/10.1175/JAS-D-15-0361.1

Liu, P., Zhao, C., Zhang, Q., Deng, Z., Huang, M., Ma, X., & Tie, X. (2009). Aircraft study of aerosol vertical distributions over Beijing and their optical properties. *Tellus B*, *61*(5), 756–767. https://doi.org/10.1111/j.1600-0889.2009.00440.x

Lyons, W. A., Nelson, T. E., Williams, E. R., Cramer, J. A., & Turner, T. R. (1998). Enhanced positive cloud-to-ground lightning in thunderstorms ingesting smoke from fires. *Science*, *282*(5386), 77–80. https://doi.org/10.1126/science.282.5386.77

MacGorman, D. R., & Rust, W. D. (1998). *The electrical nature of storms*. New York: Oxford University Press.

Malkus, J. S. (1949). Effects of wind shear on some aspects of convection. *Eos, Transactions American Geophysical Union*, *30*(1), 19–25. https://doi.org/10.1029/TR030i001p00019

Mansell, E. R., & Ziegler, C. L. (2013). Aerosol effects on simulated storm electrification and precipitation in a two-moment bulk microphysics model. *Journal of the Atmospheric Sciences*, *70*(7), 2032–2050. https://doi.org/10.1175/JAS-D-12-0264.1

Marshall, J., & Radhakant, S. (1978). Radar precipitation maps as lightning indicators. *Journal of Applied Meteorology*, *17*(2), 206–212. https://doi.org/10.1175/1520-0450(1978)017<0206:RPMALI>2.0.CO;2

McCluskey, C. S., DeMott, P. J., Prenni, A. J., Levin, E. J., McMeeking, G. R., Sullivan, A. P., et al. (2014). Characteristics of atmospheric ice nucleating particles associated with biomass burning in the US: Prescribed burns and wildfires. *Journal of Geophysical Research: Atmospheres*, *119*, 10,458–10,470. https://doi.org/10.1002/2014JD021980

Murray, B., O'sullivan, D., Atkinson, J., & Webb, M. (2012). Ice nucleation by particles immersed in supercooled cloud droplets. *Chemical Society Reviews*, *41*(19), 6519–6554. https://doi.org/10.1039/c2cs35200a

Murray, N. D., Orville, R. E., & Huffines, G. R. (2000). Effect of pollution from Central American fires on cloud-to-ground lightning in May 1998. *Geophysical Research Letters*, *27*(15), 2249–2252. https://doi.org/10.1029/2000GL011656

Niu, F., & Li, Z. (2012). Systematic variations of cloud top temperature and precipitation rate with aerosols over the global tropics. *Atmospheric Chemistry and Physics*, *12*(18), 8491–8498. https://doi.org/10.5194/acp-12-8491-2012

Omar, A. H., Winker, D. M., Vaughan, M. A., Hu, Y., Trepte, C. R., Ferrare, R. A., et al. (2009). The CALIPSO automated aerosol classification and lidar ratio selection algorithm. *Journal of Atmospheric and Oceanic Technology*, *26*(10), 1994–2014. https://doi.org/10.1175/2009JTECHA1231.1

Phillips, J., Cane, M., & Rosenzweig, C. (1998). ENSO, seasonal rainfall patterns and simulated maize yield variability in Zimbabwe. *Agricultural and Forest Meteorology*, *90*(1), 39–50. https://doi.org/10.1016/S0168-1923(97)00095-6

Proestakis, E., Kazadzis, S., Lagouvardos, K., Kotroni, V., Amiridis, V., Marinou, E., et al. (2016). Aerosols and lightning activity: The effect of vertical profile and aerosol type. *Atmospheric Research*, *182*, 243–255. https://doi.org/10.1016/j.atmosres.2016.07.031

Proestakis, E., Kazadzis, S., Lagouvardos, K., Kotroni, V., & Kazantzidis, A. (2016). Lightning activity and aerosols in the Mediterranean region. *Atmospheric Research*, *170*, 66–75. https://doi.org/10.1016/j.atmosres.2015.11.010

Randles, C. A., da Silva, A. M., Buchard, V., Darmenov, A., Colarco, P. R., Aquila, V., et al. (2016). The MERRA-2 aerosol assimilation. Technical Report Series on Global Modeling and Data Assimilation. *NASA/TM–2016-104606, 45*, 139

Ren, T., Rapp, A. D., Nasiri, S. L., Mecikalski, J. R., & Apke, J. (2018). Is the awareness of the aerosol state useful in predicting enhanced lightning for lightning-producing storms over northern Alabama? *Journal of Applied Meteorology and Climatology*, *57*(8), 1663–1681. https://doi.org/10.1175/JAMC-D-17-0182.1

Reutter, P., Su, H., Trentmann, J., Simmel, M., Rose, D., Gunthe, S., et al. (2009). Aerosol-and updraft-limited regimes of cloud droplet formation: Influence of particle number, size and hygroscopicity on the activation of cloud condensation nuclei (CCN). *Atmospheric Chemistry and Physics*, *9*(18), 7067–7080. https://doi.org/10.5194/acp-9-7067-2009

Richardson, M. S., DeMott, P. J., Kreidenweis, S. M., Cziczo, D. J., Dunlea, E. J., Jimenez, J. L., et al. (2007). Measurements of heterogeneous ice nuclei in the western United States in springtime and their relation to aerosol characteristics. *Journal of Geophysical Research*, *112*, D02209. https://doi.org/10.1029/2006JD007500

Rison, W., Thomas, R., Krehbiel, P., Hamlin, T., & Harlin, J. (1999). A GPS–based three–dimensional lightning mapping system: Initial observations in central New Mexico. *Geophysical Research Letters*, *26*(23), 3573–3576. https://doi.org/10.1029/1999GL010856

Roberts, P., & Hallett, J. (1968). A laboratory study of the ice nucleating properties of some mineral particulates. *Quarterly Journal of the Royal Meteorological Society*, *94*(399), 25–34. https://doi.org/10.1002/qj.49709540317

Rodriguez, C. A. M., da Rocha, R. P., & Bombardi, R. (2010). On the development of summer thunderstorms in the city of São Paulo: Mean meteorological characteristics and pollution effect. *Atmospheric Research*, *96*(2), 477–488. https://doi.org/10.1016/j.atmosres.2010.02.007

Ropelewski, C. F., & Halpert, M. S. (1996). Quantifying southern oscillation-precipitation relationships. *Journal of Climate*, *9*(5), 1043–1059. https://doi.org/10.1175/1520-0442(1996)009<1043:QSOPR>2.0.CO;2

Rorig, M. L., & Ferguson, S. A. (1999). Characteristics of lightning and wildland fire ignition in the Pacific Northwest. *Journal of Applied Meteorology*, *38*(11), 1565–1575. https://doi.org/10.1175/1520-0450(1999)038<1565:COLAWF>2.0.CO;2

Rosenfeld, D., Fischman, B., Zheng, Y., Goren, T., & Giguzin, D. (2014). Combined satellite and radar retrievals of drop concentration and CCN at convective cloud base. *Geophysical Research Letters*, *41*, 3259–3265. https://doi.org/10.1002/2014GL059453

Rosenfeld, D., Lohmann, U., Raga, G. B., O'Dowd, C. D., Kulmala, M., Fuzzi, S., et al. (2008). Flood or drought: how do aerosols affect precipitation? *Science*, *321*(5894), 1309–1313. https://doi.org/10.1126/science.1160606

Rosenfeld, D., Zheng, Y., Hashimshoni, E., Pöhlker, M. L., Jefferson, A., Pöhlker, C., et al. (2016). Satellite retrieval of cloud condensation nuclei concentrations by using clouds as CCN chambers. *Proceedings of the National Academy of Sciences*, *113*(21), 5828–5834. https://doi.org/10.1073/pnas.1514044113

Rotunno, R., Klemp, J. B., & Weisman, M. L. (1988). A theory for strong, long-lived squall lines. *Journal of the Atmospheric Sciences*, *45*(3), 463–485. https://doi.org/10.1175/1520-0469(1988)045<0463:ATFSLL>2.0.CO;2

Saide, P., Spak, S., Pierce, R., Otkin, J., Schaack, T., Heidinger, A., et al. (2015). Central American biomass burning smoke can increase tornado severity in the US. *Geophysical Research Letters*, *42*, 956–965. https://doi.org/10.1002/2014GL062826

Sassen, K., DeMott, P. J., Prospero, J. M., & Poellot, M. R. (2003). Saharan dust storms and indirect aerosol effects on clouds: CRYSTAL–FACE results. *Geophysical Research Letters*, *30*(12), 1633. https://doi.org/10.1029/2003GL017371

Saunders, C., Bax-Norman, H., Emersic, C., Avila, E., & Castellano, N. (2006). Laboratory studies of the effect of cloud conditions on graupel/crystal charge transfer in thunderstorm electrification. *Quarterly Journal of the Royal Meteorological Society*, *132*(621), 2653–2673. https://doi.org/10.1256/qj.05.218

Schaefer, V. J. (1949). The formation of ice crystals in the laboratory and the atmosphere. *Chemical Reviews*, *44*(2), 291–320. https://doi.org/10.1021/cr60138a004

Schultz, C. J., Carey, L. D., Schultz, E. V., & Blakeslee, R. J. (2017). Kinematic and microphysical significance of lightning jumps versus nonjump increases in total flash rate. *Weather and Forecasting*, *32*(1), 275–288. https://doi.org/10.1175/WAF-D-15-0175.1

Schultz, C. J., Petersen, W. A., & Carey, L. D. (2011). Lightning and severe weather: A comparison between total and cloud-to-ground lightning trends. *Weather and Forecasting*, *26*(5), 744–755. https://doi.org/10.1175/WAF-D-10-05026.1

Seinfeld, J. H., Bretherton, C., Carslaw, K. S., Coe, H., DeMott, P. J., Dunlea, E. J., et al. (2016). Improving our fundamental understanding of the role of aerosol−cloud interactions in the climate system. *Proceedings of the National Academy of Sciences*, *113*(21), 5781–5790. https://doi.org/10.1073/pnas.1514043113

Siu, L. W., Bowman, K. P., & Epifanio, C. C. (2015). Convective transport of trace species observed during the Stratosphere–Troposphere Analyses of Regional Transport 2008 experiment. *Journal of Geophysical Research: Atmospheres*, *120*, 10,530–10,547. https://doi.org/10.1002/2015JD023645

Smith, J., Baker, M., & Weinman, J. (2003). Do forest fires affect lightning? *Quarterly Journal of the Royal Meteorological Society*, *129*(593), 2651–2670. https://doi.org/10.1256/qj.02.175

Stevens, B., & Feingold, G. (2009). Untangling aerosol effects on clouds and precipitation in a buffered system. *Nature*, *461*(7264), 607. https://doi.org/10.1038/nature08281

Stolz, D. C., Rutledge, S. A., & Pierce, J. R. (2015). Simultaneous influences of thermodynamics and aerosols on deep convection and lightning in the tropics. *Journal of Geophysical Research: Atmospheres*, *120*, 6207–6231. https://doi.org/10.1002/2014JD023033

Stolz, D. C., Rutledge, S. A., Pierce, J. R., & Heever, S. C. (2017). A global lightning parameterization based on statistical relationships among environmental factors, aerosols, and convective clouds in the TRMM climatology. *Journal of Geophysical Research: Atmospheres*, *122*, 7461–7492. https://doi.org/10.1002/2016JD026220

Storer, R., Heever, S., & L'Ecuyer, T. (2014). Observations of aerosol–induced convective invigoration in the tropical east Atlantic. *Journal of Geophysical Research: Atmospheres*, *119*, 3963–3975. https://doi.org/10.1002/2013JD020272

Storer, R. L., Van Den Heever, S. C., & Stephens, G. L. (2010). Modeling aerosol impacts on convective storms in different environments. *Journal of the Atmospheric Sciences*, *67*(12), 3904–3915. https://doi.org/10.1175/2010JAS3363.1

Takahashi, T. (1978). Riming electrification as a charge generation mechanism in thunderstorms. *Journal of the Atmospheric Sciences*, *35*(8), 1536–1548. https://doi.org/10.1175/1520-0469(1978)035<1536:REAACG>2.0.CO;2

Tan, Y., Peng, L., Shi, Z., & Chen, H. (2016). Lightning flash density in relation to aerosol over Nanjing (China). *Atmospheric Research*, *174*, 1–8. https://doi.org/10.1016/j.atmosres.2016.01.009

Thomas, R. J., Krehbiel, P. R., Rison, W., Hunyady, S. J., Winn, W. P., Hamlin, T., & Harlin, J. (2004). Accuracy of the lightning mapping array. *Journal of Geophysical Research*, *109*, D14207. https://doi.org/10.1029/2004JD004549

Thornton, J. A., Virts, K. S., Holzworth, R. H., & Mitchell, T. P. (2017). Lightning enhancement over major oceanic shipping lanes. *Geophysical Research Letters*, *44*, 9102–9111. https://doi.org/10.1002/2017GL074982

Torres, O., Tanskanen, A., Veihelmann, B., Ahn, C., Braak, R., Bhartia, P. K., et al. (2007). Aerosols and surface UV products from Ozone Monitoring Instrument observations: An overview. *Journal of Geophysical Research*, *112*, D24S47. https://doi.org/10.1029/2007JD008809

Tuttle, J. D., Bringi, V., Orville, H., & Kopp, F. (1989). Multiparameter radar study of a microburst: Comparison with model results. *Journal of the Atmospheric Sciences*, *46*(5), 601–620. https://doi.org/10.1175/1520-0469(1989)046<0601:MRSOAM>2.0.CO;2

Twomey, S. (1959). The nuclei of natural cloud formation part II: The supersaturation in natural clouds and the variation of cloud droplet concentration. *Pure and Applied Geophysics*, *43*(1), 243–249. https://doi.org/10.1007/BF01993560

van den Heever, S. C., Carrió, G. G., Cotton, W. R., DeMott, P. J., & Prenni, A. J. (2006). Impacts of nucleating aerosol on Florida storms. Part I: Mesoscale simulations. *Journal of the Atmospheric Sciences*, *63*(7), 1752–1775. https://doi.org/10.1175/JAS3713.1

Van Donkelaar, A., Martin, R. V., Levy, R. C., da Silva, A. M., Krzyzanowski, M., Chubarova, N. E., et al. (2011). Satellite-based estimates of ground-level fine particulate matter during extreme events: A case study of the Moscow fires in 2010. *Atmospheric Environment*, *45*(34), 6225–6232. https://doi.org/10.1016/j.atmosenv.2011.07.068

Van Donkelaar, A., Martin, R. V., & Park, R. J. (2006). Estimating ground–level PM2. 5 using aerosol optical depth determined from satellite remote sensing. *Journal of Geophysical Research*, *111*, D21201. https://doi.org/10.1029/2005JD006996

Vaughan, M. A., Powell, K. A., Winker, D. M., Hostetler, C. A., Kuehn, R. E., Hunt, W. H., et al. (2009). Fully automated detection of cloud and aerosol layers in the CALIPSO lidar measurements. *Journal of Atmospheric and Oceanic Technology*, *26*(10), 2034–2050. https://doi.org/10.1175/2009JTECHA1228.1

Wang, Y., Khalizov, A., Levy, M., & Zhang, R. (2013). New directions: Light absorbing aerosols and their atmospheric impacts. *Atmospheric Environment*, *81*, 713–715. https://doi.org/10.1016/j.atmosenv.2013.09.034

Wang, Y., Lee, K.-H., Lin, Y., Levy, M., & Zhang, R. (2014). Distinct effects of anthropogenic aerosols on tropical cyclones. *Nature Climate Change*, *4*(5), 368. https://doi.org/10.1038/NCLIMATE2144

Wang, Y., Wan, Q., Meng, W., Liao, F., Tan, H., & Zhang, R. (2011). Long-term impacts of aerosols on precipitation and lightning over the Pearl River Delta megacity area in China. *Atmospheric Chemistry and Physics*, *11*(23), 12,421–12,436. https://doi.org/10.5194/acp-11-12421-2011

Wang, Y., Wang, M., Zhang, R., Ghan, S. J., Lin, Y., Hu, J., et al. (2014). Assessing the effects of anthropogenic aerosols on Pacific storm track using a multiscale global climate model. *Proceedings of the National Academy of Sciences*, *111*(19), 6894–6899. https://doi.org/10.1073/pnas.1403364111

Weisman, M. L., & Rotunno, R. (2004). "A theory for strong long-lived squall lines" revisited. *Journal of the Atmospheric Sciences*, *61*(4), 361–382. https://doi.org/10.1175/1520-0469(2004)061<0361:ATFSLS>2.0.CO;2

Wilcox, E. (2010). Stratocumulus cloud thickening beneath layers of absorbing smoke aerosol. *Atmospheric Chemistry and Physics*, *10*(23), 11,769–11,777. https://doi.org/10.5194/acp-10-11769-2010

Wilcox, E. M., Thomas, R. M., Praveen, P. S., Pistone, K., Bender, F. A.-M., & Ramanathan, V. (2016). Black carbon solar absorption suppresses turbulence in the atmospheric boundary layer. *Proceedings of the National Academy of Sciences*, 201525746. https://doi.org/10.1073/pnas.1525746113

Williams, E., & Heckman, S. (1993). The local diurnal variation of cloud electrification and the global diurnal variation of negative charge on the Earth. *Journal of Geophysical Research*, *98*(D3), 5221–5234. https://doi.org/10.1029/92JD02642

Williams, E., Mushtak, V., Rosenfeld, D., Goodman, S., & Boccippio, D. (2005). Thermodynamic conditions favorable to superlative thunderstorm updraft, mixed phase microphysics and lightning flash rate. *Atmospheric Research*, *76*(1-4), 288–306. https://doi.org/10.1016/j.atmosres.2004.11.009

Williams, E., Rosenfeld, D., Madden, N., Gerlach, J., Gears, N., Atkinson, L., et al. (2002). Contrasting convective regimes over the Amazon: Implications for cloud electrification. *Journal of Geophysical Research*, *107*(D20), 8082. https://doi.org/10.1029/2001JD000380

Williams, E., & Stanfill, S. (2002). The physical origin of the land-ocean contrast in lightning activity. *Comptes Rendus Physique*, *3*(10), 1277–1292. https://doi.org/10.1016/s1631-0705(02)01407-x

Williams, E., Weber, M., & Orville, R. (1989). The relationship between lightning type and convective state of thunderclouds. *Journal of Geophysical Research*, *94*, 13,213–13,220. https://doi.org/10.1029/JD094iD11p13213

Wilson, T. W., Ladino, L. A., Alpert, P. A., Breckels, M. N., Brooks, I. M., Browse, J., et al. (2015). A marine biogenic source of atmospheric ice-nucleating particles. *Nature*, *525*(7568), 234–238. https://doi.org/10.1038/nature14986

Wong, S., & Dessler, A. E. (2005). Suppression of deep convection over the tropical North Atlantic by the Saharan Air Layer. *Geophysical Research Letters*, *32*, L09808. https://doi.org/10.1029/2004GL022295

Wu, X., & Yanai, M. (1994). Effects of vertical wind shear on the cumulus transport of momentum: Observations and parameterization. *Journal of the Atmospheric Sciences*, *51*(12), 1640–1660. https://doi.org/10.1175/1520-0469(1994)051<1640:EOVWSO>2.0.CO;2

Yu, H., Liu, S., & Dickinson, R. (2002). Radiative effects of aerosols on the evolution of the atmospheric boundary layer. *Journal of Geophysical Research*, *107*(D12), 4142. https://doi.org/10.1029/2001JD000754

Yu, H., Zhang, Y., Chin, M., Liu, Z., Omar, A., Remer, L. A., et al. (2012). An integrated analysis of aerosol above clouds from A-Train multi-sensor measurements. *Remote Sensing of Environment*, *121*, 125–131. https://doi.org/10.1016/j.rse.2012.01.011

Yuan, T., Remer, L. A., Pickering, K. E., & Yu, H. (2011). Observational evidence of aerosol enhancement of lightning activity and convective invigoration. *Geophysical Research Letters*, *38*, L04701. https://doi.org/10.1029/2010GL046052

Yuan, T. L., Remer, L. A., Bian, H. S., Ziemke, J. R., Albrecht, R., Pickering, K. E., et al. (2012). Aerosol indirect effect on tropospheric ozone via lightning. *Journal of Geophysical Research*, *117*, D18213. https://doi.org/10.1029/2012JD017723

Zhang, Y., Gao, Z., Li, D., Li, Y., Zhang, N., Zhao, X., & Chen, J. (2014). On the computation of planetary boundary-layer height using the bulk Richardson number method. *Geoscientific Model Development*, *7*(6), 2599–2611. https://doi.org/10.5194/gmd-7-2599-2014

Zhao, B., Liou, K.-N., Gu, Y., Jiang, J. H., Li, Q., Fu, R., et al. (2018). Impact of aerosols on ice crystal size. *Atmospheric Chemistry and Physics*, *18*(2), 1065–1078. https://doi.org/10.5194/acp-18-1065-2018

Zhao, C., Liu, X., & Leung, L. R. (2012). Impact of the Desert dust on the summer monsoon system over Southwestern North America. *Atmospheric Chemistry and Physics*, *12*(8), 3717–3731. https://doi.org/10.5194/acp-12-3717-2012

Zheng, Y., Rosenfeld, D., & Li, Z. (2015). Satellite inference of thermals and cloud-base updraft speeds based on retrieved surface and cloud-base temperatures. *Journal of the Atmospheric Sciences*, *72*(6), 2411–2428. https://doi.org/10.1175/JAS-D-14-0283.1

Zipser, E. J. (1994). Deep cumulonimbus cloud systems in the tropics with and without lightning. *Monthly Weather Review*, *122*(8), 1837–1851. https://doi.org/10.1175/1520-0493(1994)122<1837:DCCSIT>2.0.CO;2

Zipser, E. J., & Lutz, K. R. (1994). The vertical profile of radar reflectivity of convective cells: A strong indicator of storm intensity and lightning probability? *Monthly Weather Review*, *122*(8), 1751–1759. https://doi.org/10.1175/1520-0493(1994)122<1751:TVPORR>2.0.CO;2